ANL/CEN/FE-79-3

ANL/CEN/FE-79-3

# SUPPORT STUDIES IN FLUIDIZED-BED COMBUSTION

## Quarterly Report
## October—December 1978

by

Irving Johnson, W. M. Swift, S. H. D. Lee,
J. A. Shearer, F. G. Teats, C. B. Turner,
W. Ira Wilson, and A. A. Jonke



U of C-AUA-USDOE

ARGONNE NATIONAL LABORATORY, ARGONNE, ILLINOIS

Prepared for the U. S. DEPARTMENT OF ENERGY
under Contract W-31-109-Eng-38

## DISCLAIMER

Printed in the United States of America
Available from
National Technical Information Service
U. S. Department of Commerce
5285 Port Royal Road
Springfield, Virginia 22161
Price: Printed Copy $5.25; Microfiche $3.00

Distribution Category:
Coal Conversion and Utilization--
Direct Combustion of Coal (UC-90e)

ANL/CEN/FE-79-3

ARGONNE NATIONAL LABORATORY
9700 South Cass Avenue
Argonne, Illinois 60439

# SUPPORT STUDIES IN FLUIDIZED-BED COMBUSTION

Quarterly Report
October—December 1978

by

Irving Johnson, W. M. Swift, S. H. D. Lee, J. A. Shearer,
F. G. Teats, C. B. Turner, W. Ira Wilson, and A. A. Jonke

Chemical Engineering Division

May 1979

Prepared for the
U.S. Department of Energy
under Contract No. W-31-109-Eng-38
and the
U.S. Environmental Protection Agency
under Agreement IAG-D5-E681



Previous reports in this series
ANL/CEN/FE-77-11
ANL/CEN/FE-78-3
ANL/CEN/FE-78-4
ANL/CEN/FE-78-10

| BIBLIOGRAPHIC DATA SHEET | 1. Report No. ANL/CEN/FE-79-3 | 2. | 3. Recipient's Accession No. |
|---|---|---|---|
| 4. Title and Subtitle<br>Support Studies in Fluidized-Bed Combustion<br>Quarterly Report, October--December 1978 | | | 5. Report Date<br>April 1979 |
| 7. Author(s)<br>I. Johnson, W. Swift S.H.D. Lee, J. Shearer, F. G. Teats, C. Turner, I. Wilson & A. A. Jonke | | | 8. Performing Organization Rept. No. ANL/CEN/FE-79-3 |
| 9. Performing Organization Name and Address<br>Argonne National Laboratory<br>9700 South Cass Avenue<br>Argonne, Illinois 60439 | | | 10. Project/Task/Work Unit No.<br>11. Contract/Grant No.<br>W-31-109-Eng-38 (DOE)<br>IAG-D5-E681 (EPA |
| 12. Sponsoring Organization Name and Address<br>U.S. Department of Energy<br>and the<br>U.S. Environmental Protection Agency | | | 13. Type of Report & Period Covered QUARTERLY<br>Oct-Dec 1978<br>14. |

15. Supplementary Notes

16. Abstracts These studies support the Fossil Energy development program in atmospheric and pressurized fluidized-bed coal combustion. Laboratory and process development-scale studies are aimed at providing needed information on limestone utilization, control of the emission of alkali metal compounds and $SO_2$ during combustion, particulate loading in flue gas, and other aspects of fluidized-bed coal combustion.

This report presents information on the effect of bed temperature, superficial gas velocity and gas hourly space velocity on the removal of gaseous NaCl from hot gas streams by a granular bed of diatomaceous earth; results of experiments in which the adsorption capacity for gaseous NaCl of activated bauxite was measured after regeneration by an aqueous leaching process; and an estimate of the cost of using these two sorbents for alkali metal control in a large PFBC. Results are also presented for studies aimed at the development of an acoustic dust conditioning system, and the evaluation of a high-efficiency cylone for removal of particles from a high-pressure high temperature gas stream. The relationship of the $SO_2$ reactivity of limestones to internal surface area, pore diameter, and pore volume are examined.

17. Key Words and Document Analysis. 17a. Descriptors

Abrasion
Additives
Air Polution
Bauxite
Calcination
Calcium Chloride
Calcium Oxides
Calcium Sulfates
Coal
Cyclone Separators
Diatomaceous Earth
Flue Gas
Fossil Fuels
Limestone
Porosity
Roasting
Sodium Chlorides
Sulfur Oxides

17b. Identifiers/Open-Ended Terms

Acoustic Dust Conditioning
Activated Bauxite
Calcium Utilization
Granular Bed Filter
Limestone Compositions
Particle Filtration
Pulse Jet-Resonant Manifold System
Sorbent Regneration
Sorbent Sulfation
Stone Structure

17c. COSATI Field/Group

| 18. Availability Statement | 19. Security Class (This Report) UNCLASSIFIED | 21. No. of Pages |
|---|---|---|
| | 20. Security Class (This Page UNCLASSIFIED | 22. Price |

TABLE OF CONTENTS

LIST OF FIGURES

LIST OF FIGURES (contd)

LIST OF TABLES

CHEMICAL ENGINEERING DIVISION

# SUPPORT STUDIES IN FLUIDIZED-BED COMBUSTION QUARTERLY REPORT

October-December 1978

by

Irving Johnson, W. M. Swift, S. H. D. Lee, J. A. Shearer, F. G. Teats, C. B. Turner, W. Ira Wilson, and A. A. Jonke

## ABSTRACT

These studies support the Fossil Energy development program in atmospheric and pressurized fluidized-bed coal combustion. Laboratory and process development-scale studies are aimed at providing needed information on limestone utilization, control of the emission of alkali metal compounds and $SO_2$ during combustion, particulate loading in flue gas, and other aspects of fluidized-bed coal combustion.

This report presents information on the effect of bed temperature, superficial gas velocity and gas hourly space velocity on the removal of gaseous NaCl from hot gas streams by a granular bed of diatomaceous earth; results of experiments in which the adsorption capacity for gaseous NaCl of activated bauxite was measured after regeneration by an aqueous leaching process; and an estimate of the cost of using these two sorbents for alkali metal control in a large PFBC. Results are also presented for studies aimed at the development of an acoustic dust conditioning system, and the evaluation of a high-efficiency cylone for removal of particles from a high-pressure high temperature gas stream. The relationship of the $SO_2$ reactivity of limestones to internal surface area, pore diameter, and pore volume are examined.

## SUMMARY

Task A. Hot Gas Cleanup

Removal of Alkali Metal Compounds from Hot Flue Gas. Methods for reducing the concentration of gaseous alkali metal compounds in hot gas are being studied. It is expected that the results of these studies will aid in the design of hot gas cleanup systems for PFBCs and help alleviate the hot corrosion of gas turbine components. The objective of the current studies is to develop the technical data base needed for the design of solid sorbent fixed-bed filters to remove gaseous alkali metal compounds from hot gas.

Previous studies demonstrated that both diatomaceous earth and activated bauxite are potentially useful sorbents for the removal of gaseous NaCl, KCl, and $K_2SO_4$ from hot gases. Effects of bed temperature, superficial gas velocity, and gas hourly space velocity were established. In the present report, results are presented which indicate that the rate of sorption of gaseous NaCl per unit quantity of diatomaceous earth is directly proportional to the concentration of NaCl in the gas phase. These studies also indicate about 90% removal of gaseous NaCl was achieved in 2- to 5-h experiments for a gas contact time of about 0.1 s and was independent of the NaCl vapor concentration in the gas.

Results are given for a series of cyclic experiments in which a sample of activated bauxite was alternately exposed to gaseous NaCl and to aqueous leaching. NaCl was sorbed during the exposure to gas and was removed during water treatment. The material regenerated by the water leaching was found to retain about 70% of its initial capacity after three cycles; this capacity is thought adequate to make use of the sorbent practical. These results indicate that activated bauxite can be regenerated and reused. Consideration of the results of these leaching experiments and the temperature dependence of the NaCl capacity of activated bauxite suggest again that in the case of activated bauxite, a large fraction of the NaCl is retained by adsorption. The mechanism of the sorption process for activated bauxite makes regeneration possible.

A preliminary estimate has indicated that the use of diatomaceous earth would add about 0.2 mill/kWh to the cost of electricity; if activated bauxite should be used but not regenerated, the added power cost would be about 1.6 mills/kWh.

Particle Removal from Flue Gas. In PFBC, the hot flue gas from the combustor must be expanded through a gas turbine to recover energy. To protect the gas turbine from damage, the particle mass loading must be reduced to acceptably low levels. Reported are (1) progress in developing a pulse-jet resonant manifold system for enhancing particulate removal by acoustic dust conditioning and (2) the results of testing a high-efficiency cyclone for particulate removal.

The effort being made at the University of Toronto (under subcontract to ANL) to develop a pulse-jet acoustic dust-conditioning system for subsequent testing and evaluation at ANL is summarized. Acoustic dust conditioning is defined as a process whereby the natural tendency of particles to agglomerate is enhanced by exposure of the particles to high-intensity acoustic fields.

The first phase of the developmental effort has been successfully completed, as signified by steady-state, continuous operation of a high-frequency, high-sound-intensity pulse jet exhausting into a tuned resonant manifold operating at ambient conditions. Sound intensities as high as 160 dB at frequencies of 300 to 350 Hz have been obtained.

Work on the second phase of the project is in progress. The objective of this phase of work is to increase the operating pressure of the pulse jet to about 1015 kPa. To date, the pulse jet has been successfully operated at pressures as high as about 350 kPa.

On the basis of the results, the pulse-jet acoustic dust-conditioning program was reassessed in terms of the basic arguments originally used to justify the development effort. Pulse-jet acoustic dust conditioning continues to look promising for PFBC applications.

The results of experiments performed to assess the particle collection efficiency of a TAN-JET cyclone are presented. The TAN-JET employs a secondary clean-air flow to improve gas-solid separation in the primary flow of dirty gas.

In experiments at ambient conditions (no combustion in the combustor), limestone was fluidized in the combustor at a gas velocity of about 0.76 m/s and a system pressure of about 250 kPa. The collection efficiency of the TAN-JET cyclone was determined from steady state determinations of (1) the cyclone (primary and TAN-JET) particle collection rates and (2) the solids loading in the flue gas downstream from the cyclone. The solids loading in the flue gas leaving the TAN-JET ranged from 0.08 to 0.17 $g/m^3$. Collection efficiency ranged from 69 to 90%. Percent penetration (100% - collection efficiency) was found to decrease with increasing mass loading in the flue gas entering the combustor. Also, the mass loading leaving the cyclone did increase with increasing mass loading entering the cyclone, an expected result.

For combustion experiments performed at 304 kPa pressure and 855°C combustion temperature, solids loading in the flue gas leaving the TAN-JET ranged from about 0.15 to about 0.24 $g/m^3$. The higher loadings than in the ambient experiments resulted from much higher inlet mass loadings to the cyclone during the combustion experiments. Under optimum secondary air inlet conditions in these experiments, mass loadings in the flue gas leaving the TAN-JET were $\geq$0.15 $g/m^3$, even with inlet mass loadings as high as about 3.2 $g/m^3$.

C. Limestone Utilization

Enhancement of Limestone Sulfation. The use of chemical additives (e.g., NaCl or $CaCl_2$) to enhance the $SO_2$ reactivity of limestones is under investigation. It has been found that salt treatment of limestones leads to larger pores when the limestone is calcined. To understand the effects of salts on the $SO_2$ reactivity of limestones, it was necessary to understand the sulfation reaction of limestones. In the present report, the relationship of the $SO_2$ reactivity of limestones with internal surface area, pore diameter, and pore volume are examined. A good correlation exists between percent conversion of $CaCO_3$ to $CaSO_4$ and the internal surface area of pores whose diameters are equal to or greater than 0.3 μm.

Results are presented which strongly suggest that very large conversions of $CaCO_3$ to $CaSO_4$ which are observed with large additions of $CaCl_2$, are due to the formation of a liquid phase which is probably a $CaCl_2$-CaO solution.

Petrographic Examination of Limestones. Petrographic analyses of several calcareous stones have been made to understand the basic structural reasons for the wide variations in $SO_2$ reactivity of different limestones. Results of the examinations of eight stones reveal no obvious structural differences correlated with their $SO_2$ reactivities.

## TASK A. HOT GAS CLEANUP

### 1. Removal of Alkali Metal Compounds from Hot Flue Gas of Coal Combustion (S. H. D. Lee)

In the prospective application of pressurized fluidized-bed combustion of coal to power generation, the corrosion of turbine blades due to attack by alkali metal compounds in the hot flue gas is a potential problem. This problem can be eliminated by reducing the concentration of alkali metal compounds in the hot flue gas to a level tolerable for a turbine blade. A way to accomplish this is to use a hot fixed-bed filter having a sorbent as bed material to remove the alkali metal compounds from the hot flue gas before the gas is expanded into a turbine. The objective of this task is to develop an effective sorbent as bed material for the filter.

Previous experiments have shown that both diatomaceous earth and activated bauxite effectively remove NaCl, KCl, and $K_2SO_4$ vapors from the simulated hot flue gas of PFBC. The effects of sorbent bed temperature, superficial gas velocity, and gas hourly space velocity of flue gas were studied and were presented (ANL/CEN/FE-78-10). During the present report period, studies have been continued (1) to investigate the effect of NaCl vapor concentration in flue gas on the sorption efficiency of diatomaceous earth, (2) to examine the regenerability of activated bauxite by a water-leaching process, and (3) to gain a better understanding of the sorption mechanisms of NaCl vapor by these two sorbents. Also, a preliminary economic evaluation was made of both diatomaceous earth and activated bauxite as sorbents for the removal of alkali metal compounds from hot flue gas of PFBC. Results of the above studies and the preliminary economic evaluation are presented and discusssed.

#### a. Effect of NaCl Vapor Concentration in Flue Gas on the Sorption Efficiency of Diatomaceous Earth

Except for screening tests with $K_2SO_4$ vapor, tests completed so far were generally conducted by feeding a simulated flue gas of PFBC containing about 80 ppm alkali metal compound vapor. Alkali concentration in the flue gas of PFBC has been estimated to be of the order of 10 ppm.

In order to investigate the effect of NaCl vapor concentration in the flue gas on the sorption efficiency of diatomaceous earth, a series of experiments was carried out in a laboratory-scale, batch-unit combustor,* using simulated flue gas (3%$O_2$, 16%$CO_2$, about 300 ppm $SO_2$, about 120 ppm $H_2O$, and the balance $N_2$) containing about 29 ppm NaCl vapor. A detailed description of the combustor was presented in an earlier report in this series (ANL/ES-CEN-1016). In these experiments, diatomaceous earth sorbent was tested at 800°C and atmospheric pressure as a function of experiment duration. The

---

* The combustion system consists of a horizontal tube furnace and associated gas feed lines and product gas analysis instrumentation. The first sector of the tube furnace is a gas preheater; the next sector contains a sample pan which can be heated along with its contents; next is a granular bed sorbent filter, followed by cold traps and a backup glass wool filter.

superficial gas velocity and the gas hourly space velocity (GHSV) of simulated flue gas passing through the sorbent bed were 66 cm/s and 33,500 $h^{-1}$, respectively. Particles were -8 +10 mesh. The distributions of NaCl obtained from these experiments are tabulated in Table 1, and the results are plotted in Figs. 1 and 2. To allow comparison of the effects of two NaCl conentrations, the results of a test run (Experiment HGC-47) conducted at the same experimental conditions except with a 96 ppm NaCl concentration in the simulated flue gas are also included in the table and the figures.

Figure 1 is a plot of the rate of NaCl vapor sorption by diatomaceous earth in milligrams NaCl per gram of sorbent per hour as a function of NaCl concentration in the simulated flue gas (in parts per million). Except for the 8-h run, all points fit excellently on a straight line passing through the origin of the scale. This indicates that at the experimental conditions used, the rate of NaCl vapor sorption by diatomaceous earth is a linear function of the NaCl vapor concentration in the simulated flue gas for the initial few hours of the tests.

Figure 2 is a plot of the percent of NaCl vapor in flue gas captured by diatomaceous earth as a function of experiment duration. At an average NaCl vapor concentration of 29 ppm in the simulated flue gas and with a fairly high space velocity of 33,500 $h^{-1}$ (which is equivalent to a contact time of about 0.1 s for the simulated flue gas and the sorbent bed), the efficiency with which diatomaceous earth removes NaCl vapor from the simulated flue gas approaches 90% for tests no longer than 5 h. It should be noted that the efficiency can be increased by reducing the space velocity of the simulated flue gas or by increasing the contact time of the simulated flue gas and the sorbent bed. Comparison of the capture efficiences obtained at the low NaCl vapor concentration with that at the high NaCl vapor concentration (Fig. 2) shows that the efficiency with which diatomaceous earth removes NaCl vapor from the simulated flue gas is not affected at those NaCl vapor concentrations in the flue gas.

b. NaCl Adsorption and Water-Leaching Regeneration of Activated Bauxite Sorbent

A three-cycle experiment of (1) NaCl adsorption and (2) regeneration of activated bauxite by water leaching were completed. The adsorption test was carried out using the small-scale adsorption test rig that has been shown and described in detail previously (ANL/CEN/FE-78-4). Figure 3 is a flow sheet diagram showing the experimental steps for this set of experiments, as well as the manner of determining material balances.

Physical Observations. Fresh activated bauxite is light pink. When it is exposed to NaCl vapor and has adsorbed it, the bauxite becomes milky white. However, after the NaCl-adsorbed activated bauxite is leached with water and dried in a furnace, the original light-pink color is restored. This color-change phenomenon was observed in all three cycles of adsorption and regeneration experiments--the adsorption of NaCl vapor (which is milky white when condensed) on the surface of activated bauxite during the adsorption stage was indicated, as was, the release of NaCl from the surface during the water-leaching regeneration step. The latter argument is confirmed by the analytical results (presented below) showing mole ratio of $Na^+$ to $Cl^-$ of unity in the leachants.

Table 1. Distributions of NaCl from testing Diatomaceous Earth for NaCl Vapor Capture as a Function of Experimental Duration and NaCl Concentration in the Simulated Flue Gas. Sorbent (-8 +10 mesh) was tested at 800°C and atmospheric pressure in a simulated flue gas of PFBC at a linear gas velocity of 66 cm/s and GHSV of 33,500 $h^{-1}$.

| | HGC-47 | HGC-57 | HGC-57R | HGC-58 | HGC-58R | HGC-56 | HGC-62 | HGC-55 |
|---|---|---|---|---|---|---|---|---|
| Experiment Duration, h | 2 | 2 | 2 | 3 | 3 | 5 | 5 | 8 |
| Avg NaCl Conc. in Simulated Flue Gas to the Filter, ppm | 96 | 37 | 24 | 33 | 28 | 27 | 27 | 29 |
| Amount of Sorb., g | 30 | 13 | 13 | 13 | 13 | 13 | 13 | 13 |
| (1) NaCl, mg, Collected by: | | | | | | | | |
| (a) Cold Trap | 29 | 5 | 3 | 4 | 7 | 7 | 11 | 51 |
| (b) Glass-wool Filter | 18 | 2 | 2 | 1 | 3 | 3 | 5 | 22 |
| (2) NaCl Captured by: Sorb.,[a] mg | 292 | 49 | 31 | 66 | 57 | 90 | 89 | 104 |
| (3) Total NaCl, mg | 339 | 56 | 36 | 71 | 67 | 100 | 105 | 177 |
| (4) Rate of Sorption, mg NaCl/h-g sorb. | 4.9 | 1.9 | 1.2 | 1.7 | 1.5 | 1.4 | 1.4 | 1.0 |
| (5) % NaCl Capture, [(2)/(3)]x100 | 36.1 | 87.5 | 86.1 | 93.0 | 85.1 | 90 | 84.8 | 58.8 |

[a] NaCl concentration of the sorbent was obtained by dissolving representative samples of the sorbent in a mixture of $H_2SO_4$, HF, and $HNO_3$, and then analyzing the solution by flame emission spectrometry (FE). FE analysis was done by R. Bane.

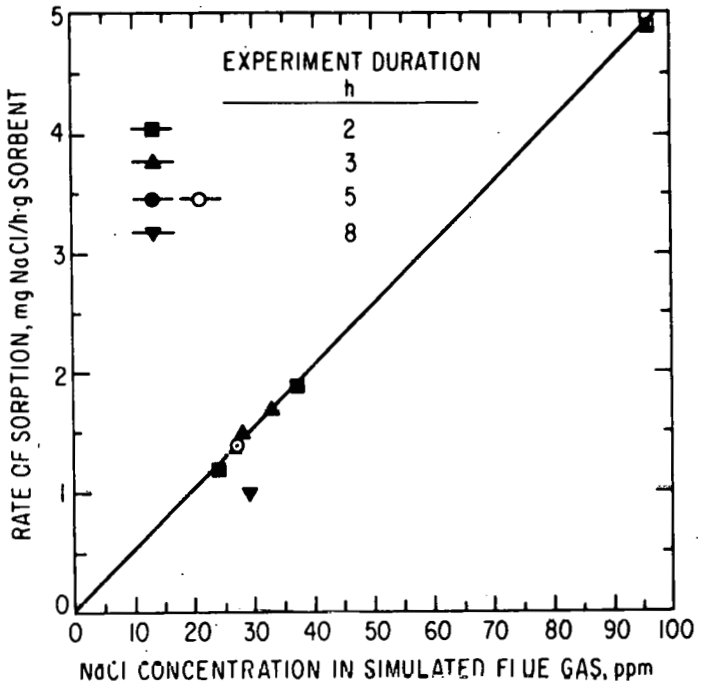


Fig. 1. Rate of NaCl Sorption by Diatomaceous Earth as a Function of NaCl Concentration in Simulated Flue Gas Transported to the Sorbent Bed.

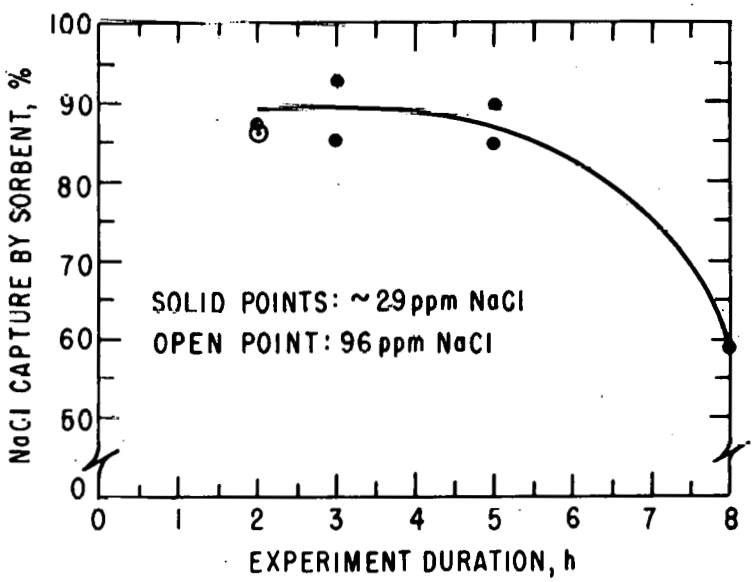


Fig. 2. Effect of NaCl Concentration in Simulated Flue Gas on NaCl Capture by Diatomaceous Earth as a Function of Experiment Duration. GHSV = 33,500 $h^{-1}$

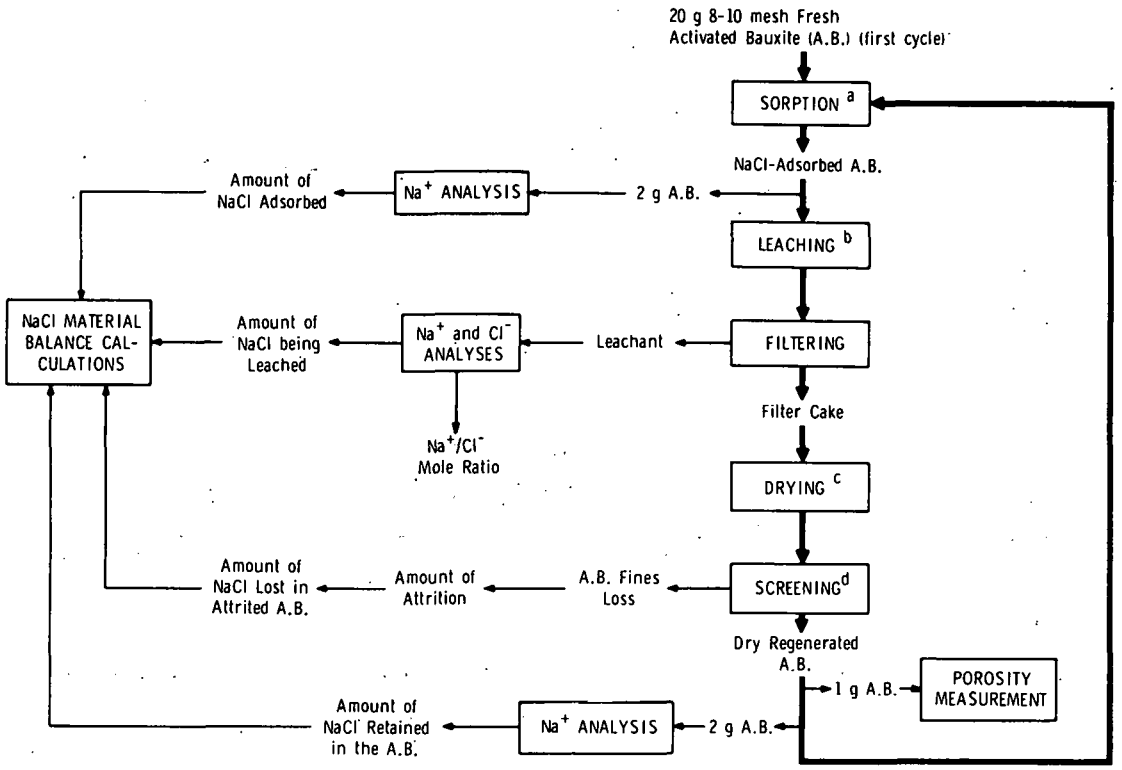


Fig. 3. Flow Sheet Showing a NaCl Adsorption and Water-Leaching Process and Analyses for Activated Bauxite.

a. Sorption Conditions: 800°C and atmospheric pressure in a simulated flue gas of PFBC containing 3% $O_2$, 16% $CO_2$, about 300 ppm $SO_2$, about 120 ppm $H_2O$, about 220 ppm NaCl vapor, and the balance $N_2$. The linear velocity of flue gas passing through the bed was 27 cm/s. The experiment duration was 2 h.
b. Leaching Conditions: Distilled water leaching at gently boiling temperature (about 95°C) for 1 h.
c. Drying Conditions: 200°C for 2 h in an air flow.
d. Screened with 14-mesh screen.

Porosity Measurement of Sorbents. Figure 4 shows a plot of cumulative pore volume as a function of pore diameter for both fresh and regenerated activated bauxites. It can be seen from this figure that in comparison to fresh activated bauxite, the regenerated activated bauxites lost a small amount of large pores (>2 μm); however, they gained fair amounts of pore volume in the very fine pores (<0.06 μm). The pore volume continued to increase in later regeneration cycles. Internal surface area is essential for the adsorption process and is mainly contributed by small pores; therefore, the increase of fine pores of the regenerated activated bauxite should increase its internal surface area and thus its adsorption capacity.

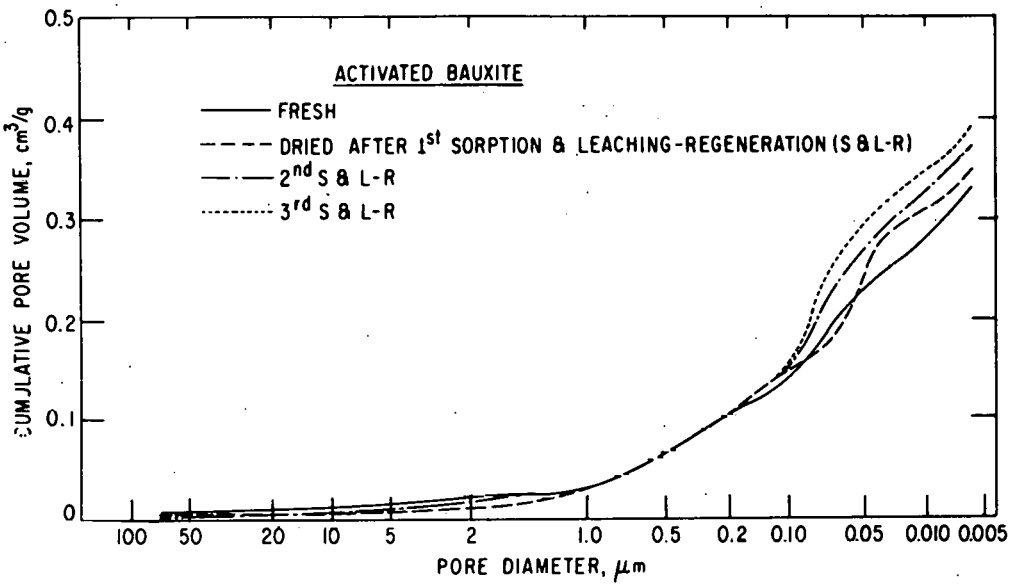


Fig. 4. Cumulative Pore Volume as a Function of Pore Diameter for Activated Bauxites on which NaCl was Sorbed followed by Regeneration (i.e., Water Leaching).

Attrition of Sorbent. During the water-leaching regeneration stage, activated bauxite fines were produced due to attrition of the sample. The amount of attrition not only is an indication of the resistance to abrasion of the sample but also more importantly allows sample loss during the water-leaching regeneration process to be estimated. Table 2 gives the attrition, in percent, of activated bauxite caused by water-leaching regeneration for each of the three cycles. Attrition was 6.6% in the first cycle and decreased to 2.8% in the third cycle.

Table 2. Attrition of Activated Bauxite Caused by Three Cycles of Water Leaching (Regeneration). NaCl-adsorbed activated bauxite (A.B.) was leached with distilled water at gently boiling temperature (~95°C) for 1 h.

| Cycle of Leaching | Wt. of A.B. Leached,[a] g | Wt. of A.B. Lost[b] as Fines, g | Attrition, % |
|---|---|---|---|
| 1 | 18.5725 | 1.2304 | 6.6 |
| 2 | 11.2877 | 0.3397 | 3.0 |
| 3 | 4.6802 | 0.1324 | 2.8 |

[a]The weight of activated bauxite has been corrected for the weight of NaCl that was leached out.

[b]Includes all particles passing through a 14-mesh screen.

Leachant Analysis. Previous experimental results (Table 5, ANL/CEN/FE-77-11) indicated that sodium and chloride ions were present in the water leachant from NaCl-adsorbed activated buxite in about equal concentrations. To further confirm the earlier results, the leachants from all three cycles of water-leaching regeneration in this investigation were analyzed for $Na^+$ and $Cl^-$ concentration. The analytical results are tabulated in Table 3. As shown in the right-hand column of the table, within the limits of analytical and experimental error, the mole ratio of $Na^+$ to $Cl^-$ is approximately unity for all three leachants. These results confirm the previous results, as well as the conclusion that the leachable NaCl is retained by activated bauxite by an adsorption process. It can also be observed in Table 3 that at later leaching cycles, higher concentrations of $Na^+$ and $Cl^-$ are leached (on the basis of moles per gram of activated bauxite), indicating that the adsorption process plays an increasing role in NaCl vapor capture by activated bauxite. The role of the adsorption process in NaCl vapor capture by activated bauxite (as compared with another NaCl-retention mechanism) is discussed next.

Table 3. Concentrations of Sodium and Chloride Ions in the Leachants from Water-Leaching Regeneration of NaCl-Adsorbed on Activated Bauxite. NaCl-adsorbed activated bauxite was leached with distilled water at gently boiling temperature (∿95°C) for 1 h.

| Cycle of Leaching | Wt. of Sample Leached, g | Ion Concentration in Leachant, mmol/g sample | | $Na^+/Cl^-$ Mole Ratio |
|---|---|---|---|---|
| | | $Na^+$ | $Cl^-$ | |
| 1 | 18.5830 | 0.22 | 0.23 | 0.96 |
| 2 | 11.2949 | 0.25 | 0.23 | 1.09 |
| 3 | 4.6833 | 0.26 | 0.24 | 1.08 |

NaCl Material Balances. By the procedure described in Fig. 3, the amounts of NaCl (1) adsorbed during the adsorption stage, (2) leached out during the water-leaching regeneration stage, (3) lost in attrited activated bauxite, and (4) retained in the activated bauxite were determined. A material balance of NaCl was made for each cycle. Table 4 shows the results. The NaCl material balances shown in the first row in the table were calculated in units of milligrams per gram of activated bauxite and also represent the sorption capacities.

As can be seen in the table, very good material balances were obtained for all three cycles of the experiment. For the first cycle, 24.2 mg NaCl was captured per gram of activated bauxite.

Of the amount of NaCl captured, about 51% was leached out during water-leaching regeneration. In other words, about 51% of the NaCl captured by activated bauxite was captured by an adsorption process. The remainder of the NaCl captured (about 49%) was retained in the activated bauxite. Bauxite is a principal ore of aluminum, and consists mainly of aluminum oxide and impurities including $SiO_2$ and clay minerals. Activated bauxite used for this study contains 81% $Al_2O_3$ and 10% $SiO_2$. The reactions of NaCl with the $SiO_2$ and the clay minerals in the activated bauxite are believed responsible for retention of the about 49% of NaCl captured.

Table 4. NaCl Material Balances for (1) NaCl-Vapor Adsorption and (2) Water-Leaching Regeneration of Activated Bauxite (A.B.)

| | NaCl, mg/g Activated Bauxite | | |
|---|---|---|---|
| | Cycle 1 | Cycle 2 | Cycle 3 |
| INPUT | | | |
| (1) NaCl Adsorbed[a] (i.e., sorption capacity) | 24.2 | 22.2 | 16.6 |
| OUTPUT | | | |
| (2) NaCl Leached out | 12.3(50.8%) | 14.7(66.2%) | 14.8(89.2%) |
| (3) NaCl Retained in A.B.[b] after Leaching | 10.4(43.0%) | 6.5(29.3%) | 1.4(8.4%) |
| (4) NaCl Lost in Attrited Material after Leaching | 0.7(2.9%) | 0.5(2.3%) | 0.5(3.0%) |
| (5) Total | 23.4 | 21.7 | 16.7 |
| (6) Loss [(1)-(5)] | 0.8(3.3%) | 0.5(2.2%) | -0.1(-0.6%) |

[a] Except for the first cycle, the values were obtained by subtracting the amount of NaCl retained in the dry regenerated activated bauxite (row 3) of the previous cycle from the total NaCl in the NaCl-adsorbed activated bauxite.

[b] Except for the first cycle, the values were obtained by subtracting the amount of NaCl retained in the dry regenerated activated bauxite (row 3) of the previous cycle from the total NaCl in the dry regenerated activated bauxite.

In the second and third cycles, the sorption capacities (row 1) decreased to about 92% and about 70% of the sorption capacity achieved in the first cycle. This decrease in sorption capacity is due to the loss of the chemical reactivity with the $SiO_2$ and clay minerals in the activated bauxite. However, it may be seen in row 2 of Table 4 that the quantity of NaCl captured by an adsorption process increases in the second and third cycles. This is believed to be due to an increase in the internal surface area of the regenerated activated bauxite, as discussed previously. In contrast to the greater

NaCl capture by an adsorption process in the second and third cycles, NaCl capture by chemical reactions with $SiO_2$ and clay minerals decreased sharply in the later cycles (row 3 of Table 4).

On the basis of these data, it can be reasonably inferred that after third-cycle regeneration, NaCl vapor will be captured by activated bauxite essentially by an adsorption process. An adsorption process is a reversible process, which means that the adsorbent can be reused repeatedly after desorptions of the adsorbate. For a given adsorbate and for unit weight of a given adsorbent, the amount of adsorbate adsorbed at equilibrium is a function of the final pressure and temperature only;[1] therefore, after the third cycle, at constant pressure and temperature, the amount of NaCl vapor adsorbed (i.e., the sorption capacity) by activated bauxite through a pure adsorption process should be constant and independent of adsorption and regeneration cycle. Based on this behavior, the sorption capacity of about 16 mg NaCl per gram activated bauxite would be maintained starting with the fourth cycle of the sorption and regeneration process.

Under different conditions, the sorption capacities obtained for activated bauxites using the laboratory-scale batch-unit fixed-bed combustor on a once-through basis were smaller than 8 mg NaCl per gram of activated bauxite; greater than 90% of the NaCl vapor was removed from simulated flue gas of PFBC (ANL/CEN/FE-78-10). Therefore, since 90% of the NaCl could be removed using fresh activated bauxite which captured only 8 mg NaCl per gram, the adsorption capacity of 16 mg NaCl per gram of regenerated activated bauxite is very adequate for a practical application, with greater than 90% removal of NaCl vapor from flue gas achievable.

On the basis of experimental results obtained from this adsorption and water-leaching regeneration experiment, it can be concluded that activated bauxite can be easily regenerated and reused by a simple water-leaching process.

### c. Mechanisms of Sorption of NaCl Vapor by Diatomaceous Earth and Activated Bauxite

Diatomaceous earth is a sedimentary rock of marine or lacustrine deposition. Chemically, it consists primarily of silicon dioxide and various amounts of impurities such as clay, carbonaceous matter, iron oxide, sand, etc. Celatom MP-91 diatomaceous earth is a product of Eagle-Picher Industries, Inc., Ohio, and is used in this study. It contains 92% $SiO_2$, 5% $Al_2O_3$, and other impurities. Previous experimental results (Table 5, ANL/CEN/FE-77-11) from this work indicated that NaCl vapor captured by diatomaceous earth was primarily tied up in chemical forms that are not soluble in water. The reaction of

$$2\ NaCl(g) + H_2O(g) + n\ SiO_2(s) = Na_2O \cdot n\ SiO_2(s) + 2\ HCl(g)$$

$$\Delta H_{1073K} = 5.71\ \text{kcal mol}^{-1} \text{ for } n = 1$$

is well known and has been studied.[2,3] The NaCl vapor retained by diatomaceous earth is believed to primarily react with diatomacous earth according to the above reaction to form sodium silicates that are not readily soluble

in water. The solubility of an alkali metal silicate depends on the ratio of silica to alkali metal oxide and is also controlled by the amount of impurity present.[4] Part of the NaCl vapor may also react with clays present as impurities in diatomaceous earth because clay minerals are known to be effective "getters" for alkali metal compounds.[5-7] In an investigation of the kinetics of the above reaction, it was reported[3,8] that between 840 and 940°C, the rate of the above reaction increases with temperature according to the Arrhenius equation. The rate of reaction of NaCl vapor with diatomaceous earth in the present system is also noted to increase with temperature (ANL/CEN/FE-78-10).

Bauxite is a principal ore of aluminum; it consists mainly of aluminum oxide and other impurities, including $SiO_2$ and clay minerals. As shown and discussed in Section 1.b. of this task (NaCl Adsorption and Water-Leaching Regeneration of Activated Bauxite Sorbent), 51% of the NaCl vapor is captured by activated bauxite by an adsorption process for the fresh activated bauxite. In contrast to the chemical process (reactions of NaCl vapor with $SiO_2$ and clay minerals in activated bauxite), adsorption sharply increases at later regeneration cycles.

d. Preliminary Economical Evaluations of Diatomaceous Earth and Activated Bauxite used for the Removal of Alkali Metal Compounds from Hot Flue Gas of PFBC

Both diatomaceous earth and activated bauxite (alkali sorbents) are effective in removing alkali metal compounds from hot simulated flue gas of PFBC, as has been experimentally demonstrated. Here, these two alkali sorbents are further evaluated from a practical economic viewpoint. To allow comparison, the cost of $SO_2$ sorbent is also included in this evaluation. Table 5 shows assumptions and computation bases for this preliminary economic evaluation for a 200-MWe PFBC demonstration plant.

On the basis of assumptions in Table 5, a material balance around a 200-MWe PFBC demonstration plant combustor was made and is shown in Fig. 5. The material balance shows that 206.9 ML/h flue gas at 800°C and 1 MPa (10 atm) will be produced which must be treated for removal of alkali metals. Experimental results showed that both diatomaceous earth and activated bauxite can achieve 90% removal of alkali metals from the flue gas at a gas hourly space velocity (GHSV) of 33,500 $h^{-1}$. The GHSV is defined as the volumetric flow rate of flue gas per units of sorbent volume per hour. Therefore, the volumetric flow rates of alkali sorbents required to treat 206.9 ML/h flue gas can be calculated. With known bulk densities and current prices of alkali sorbents, as shown in Table 5, the mass flow rate of alkali-sorbents needed and also the cost of the sorbents for a given mass flow rate of coal burned can be computed. Table 6 shows the computed results.

As compared with the 0.82 mill cost for $SO_2$ sorbent per kWe-h electricity produced, 0.22 and 1.64 mill would be the costs of using diatomaceous earth and activated bauxite, respectively, to achieve 90% removal of alkalis from the hot flue gas from a 200-MWe PFBC demonstration plant. Although the cost of using activated bauxite is about eight times the cost of diatomaceous earth, this cost differential may be offset by regeneration of activated bauxite.

Table 5. Assumptions and Computation Bases for the Preliminary Economic Evaluations of Granular Sorbents (Diatomaceous Earth and Activated Bauxite) for the Removal of Alkali Metal Compounds from Hot Flue Gas of a 200-MWe PFBC Demonstration Plant

Assumptions for 200-MWe PFBC Demonstration Plant

(1) Coal: Typical Illinois coal with a heating value of 29 MJ/kg of coal (12,500 Btu/lb) and an ultimate analysis of 70.3% C, 5.0% H, 1.3% N, 3.3% S, 11.4% ash, and 8.7% O.

(2) $SO_2$ Sorbent: Tymochtee dolomite containing 51.8% $CaCO_3$ (20.7% Ca) and 43.3% $MgCO_3$; once-through operation.

(3) Excess Air: 20%

(4) Ca/S Mole Ratio for 80% S removal: 1.5

(5) Over-all Cycle Efficiency: 40%

Computation Bases for Alkali-Sorbent Evaluation

(1) 90% removal of alkali metal compounds from hot flue gas (800°C) assumed to contain 29 ppm (by vol) alkalis at linear velocity of 66 cm/s (2.2 ft/s) and GHSV = 33,500 $h^{-1}$ (This basis is achievable based on the experimental results obtained with both diatomaceous earth and activated bauxite at 800°C and atmospheric pressure operations)

(2) Bulk Density of Granular Sorbents ($\rho$ given by manufacturer)

$\rho_{D.E.}$ = 24 lb/$ft^3$ (385 g/L)

$\rho_{A.B.}$ = 55 lb/$ft^3$ (882 g/L)

(3) Current Price of Granular Sorbents (August 1978)

$80/ton of diatomaceous earth

$275/ton of activated bauxite

$8/ton of $SO_2$ sorbent (assumed)

(4) Once-through operation for alkali sorbents

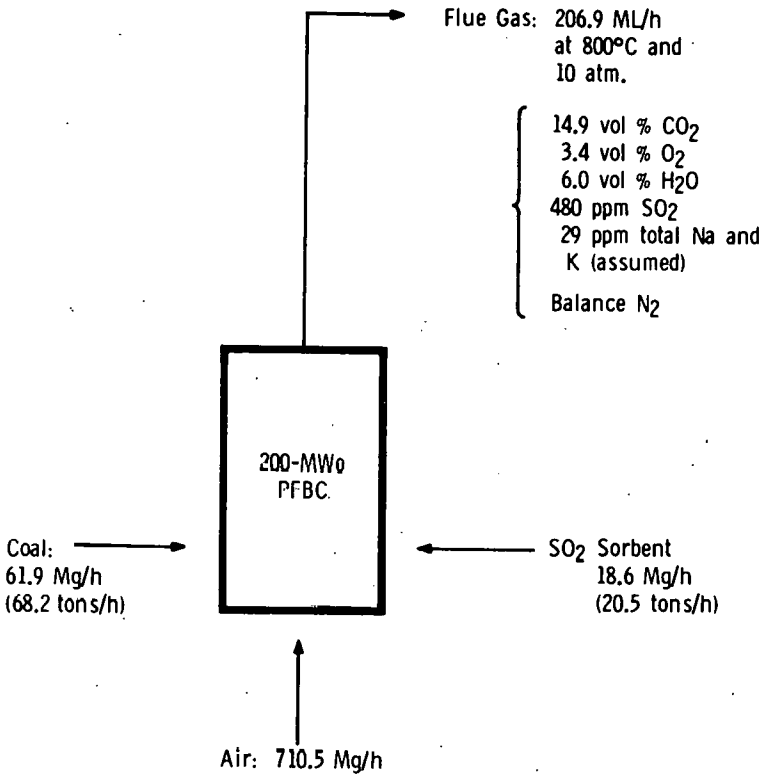


Fig. 5. Material Balance for Conceptual 200-MWe PFBC Demonstration Plant, based on Assumptions in Table 5.

Table 6. Granular Sorbents for Removal of Alkalis and $SO^2$, 200-MWe PFBC Demonstration Plant. Calculations are based on assumptions and computation bases in Table 5.

| Sorbent | Sorbent Required per ton of Coal Burned, lb | Cost of Sorbent per ton, $ | Cost of Sorbent per kWe-h Produced, mill/kWe-h |
|---|---|---|---|
| $SO^2$ Sorbent | 601 | 8 | 0.82 |
| Diatomaceous Earth | 16 | 80 | 0.22 |
| Activated Bauxite | 35 | 275 | 1.64 |

It is emphasized that the results presented in Table 6 were computed on the basis of removing 90% of the alkali metal compounds from hot flue gas which is assumed to contain 29 ppm alkali vapors. This basis was chosen because with both diatomaceous earth and activated bauxite, 90% alkali removal from hot simulated flue gas of PFBC containing 29 ppm NaCl vapor had been achieved experimentally at 800°C and atmospheric-pressure operation. To the present, however, no reliable measurement of the level of total alkali in the flue gas of PFBC has been obtained, nor is the allowable level of alkalis in the flue gas of PFBC that is tolerable by a gas turbine known. Based on thermodynamic calculations made by researchers at General Electric Company, it has been estimated that the alkali vapor present in the flue gas of PFBC will approach 10 ppm when coal containing 0.1% Cl is combusted at 950°C. Based on experience with gas turbine liquid fuel, that level of alkali vapor may be as much as two orders of magnitude greater than the acceptable limit of a gas turbine.[9] On the basis of this information, the acceptable limit of a gas turbine may not be met by removing only 90% of alkalis from flue gas. However, with both diatomaceous earth and activated bauxite, higher removal efficiency can theoretically be achieved at high pressure (10 atm) and longer contact time or shorter GHSV (<33,500). Further experiments are needed to investigate the performance of the two alkali sorbents at high pressures and low concentrations of alkali vapor in the flue gas.

## 2. Particle Removal from Flue Gas

(W. M. Swift, F. G. Teats, A. R. Pumphrey, S. D. Smith, and J. J. Stockbar)

In PFBC, the hot flue gas from the combustor must be expanded through a gas turbine to recover energy and make the process economic. However, to prevent erosion of the turbine blades by particles of limestone and fly ash entrained in the flue gas, the particle mass loading must be reduced to acceptably low levels.

Although the air quality requirements for a gas turbine have yet to be experimentally demonstrated, estimates have been made of what constitute "acceptably low levels" of particle mass loading for a gas turbine. Westinghouse, for example, has suggested that loadings in the range of about 0.05 to about 0.005 $g/m^3$ (depending on the particle size distribution) would be acceptable.[10] Since particle loadings in the flue gas leaving the combustor are on the order of about 30 $g/m^3$, a total particle-removal efficiency between 99.8 and 99.98% would be needed to meet the turbine air-quality requirements.

Existing devices readily adaptable to high-temperature, high-pressure particle removal such as conventional cyclones are not very efficient in removing particles having diameters smaller than about 10 μm. Thus, achieving the very low loadings necessary for PFBC requires that highly efficient methods be developed for removing particles having diameters between 2 and 10 μm from high-temperature/high-pressure flue gas.

Promising flue-gas cleaning methods identified for testing and evaluation in the off-gas system of the ANL 15.2-cm-dia fluidized-bed combustor include granular-bed filtration, high-efficiency cyclones, and acoustic agglomeration. This report presents (1) the progress made in developing a pulse-jet resonant-manifold system for investigation of acoustic dust conditioning and (2) the results of testing a high-efficiency cyclone.

### a. Acoustic Dust Conditioning

Acoustic dust conditioning (ADC) is a technique to enhance the natural tendency of polydispersed particles to impact upon each other and agglomerate. Fine particle emissions are controlled in a process whereby the mean size of the effluent particles is significantly increased by exposure to high-intensity finite-amplitude acoustic fields. Acoustic dust conditioning would be incorporated into the off-gas treatment system to increase the collection efficiency of downstream dust collectors.

Efforts to date for development and fabrication of a pulse-jet acoustic dust conditioning (PJ-ADC) system have been carried out (under a subcontract) at the University of Toronto.* Components of the system (ANL/CEN/FE-78-4, p. 35) include (1) a pulse-jet sound generator, (2) a resonant manifold system to match the acoustic system capacity with the FBC system volumetric gas flow capacity, and (3) an acoustic treatment section where the flue gas can be exposed to the acoustic field.

*Direction is by Dr. David S. Scott, Professor and Chairman, Department of Mechanical Engineering.

The merits of PJ-ADC as applied to PFBC have been reviewed,[11] and the basic reasoning supporting the development effort is repeated here:

1. PJ-ADC at ambient atmospheric conditions has achieved 5- to 7-fold increases in the mean particle diameter of industrial type aerosols.[12] Qualitative arguments involving primarily interparticle spacing but not particle-particle adhesion, indicate that at the expected temperatures and pressures of PFBC, ADC should be even more effective than at ambient conditions.

2. Performance evaluations indicate that high-efficiency cyclones may reduce solids loadings sufficiently to meet the gas turbine inlet criterion for particle loading if the mean particle diameter entering the cyclone is increased by a factor of 2 to 5.[13]

3. Pulse jets are combustors, and exhausting the heat of combustion from pulse jets directly into the off-gases from the PFBC would add to the internal energy of the flue gas. This heat would be extractable by the turbine with the same efficiency as the PFBC heat of combustion extracted from the flue gas. Thus, in principle, the power cost chargeable to particle gas separation by PJ-ADC would be very nearly zero.

4. Qualitative arguments indicate that pulse jets should yield higher powers and higher efficiencies when run at pressures greater than atmospheric.

5. The capital and operating costs for PJ-ADC are expected to be very low. Thus, the use of PJ-ADC could be very advantageous in whatever particle/gas separation technology is employed (high-efficiency cyclone, granular-bed filter, or ceramic fabric filter are examples).

The effort at the University of Toronto was divided into three phases: Phase I, the design, fabrication, and testing of a pulse jet-resonant manifold system (PJ-RMS) at atmospheric pressure, has been completed. Phase II, increasing the operating pressure of the PJ-RMS to about 1.01 MPa, has been initiated. Phase III, which is to be the design, manufacture, and testing of a PJ-RMS system for installation and evaluation in the flue gas system of the ANL fluidized-bed combustion process development unit, is yet to be initiated.

The results of the work at the University of Toronto have been very encouraging. Major uncertainties surrounding the development of the PJ-RMS have been removed, and the effort has yielded no evidence that the technical objectives of the project cannot be met. However, the project has required significantly more developmental work than was originally anticipated. The results obtained to date are summarized below. Emphasized are the advances made in pulse jet technology during the developmental effort.

Phase I. Phase I was completed, signified by the steady state, continuous operation of a high-frequency, high-sound-intensity pulse jet exhausting into a tuned resonant manifold operating at approximately ambient conditions. Sound intensities as high as 160 dB were achieved while frequencies of about 300 Hz were maintained.

Prior to the initiation of this project, the University of Toronto had benefitted from the experience of developing pulse jets for ADC evaluations in various prototype projects conducted at Ontario Research Foundation.[12] However, the specific pulse jets used at Ontario Research Foundation were not well suited to the requirements of PFBC. To provide the necessary technical background for pulse-jet development as part of the ANL project, an extensive review of the literature was first undertaken.

For reasons of both safety and convenience, propane was selected as the fuel for the pulse jet during development. Although other fuels have not been used in the developmental program, almost any fuel can in principal be adapted to PJ operation--even pulverized coal.

The first PJ configurations examined in this study operated at intensities up to 130 dB and at frequencies up to 295 Hz, with the microphone placed at a relatively arbitrary location (at a 45° angle approximately 15 cm from the opening of the PJ exhausting tail-pipe.) In an intensive program of pulse-jet upgrading, units were developed which achieved sound intensities as high as 160 dB at a frequency of 280 Hz. During this development, dimensional and configurational changes were made in the combustion chamber, exhaust pipe, and air/fuel mixing and inlet designs. Furthermore, air- and water-cooling systems were developed for control of the metal temperatures of the combustion chamber and exhaust pipe, respectively.

After acceptable performance of the pulse-jet was achieved, testing of the pulse jet exhausting into a resonant manifold was initiated. Tuned as a length resonator, the combined PJ-RMS exhibited the capability of producing greater total sound power, as well as higher frequencies, than could the same pulse jet exhausting into the free atmosphere. It was also discovered that a "double-frequency" operating mode could be achieved (about 550 Hz) by proper adjustment of the overall length of the resonant manifold. At these "double frequencies," higher sound levels were achieved than with normal RMS frequencies of about 300 Hz.

Although the absence of definitive and quantitiative diagnostics prevents unequivocal claims regarding pulse-jet performance, the following are claimed as advances in pulse-jet technology:

1. The achievement of sound intensity levels of about 160 dB, as measured at the location indicated above, at a frequency of about 300 Hz is believed to exceed the highest sound levels previously obtained at this frequency by pulse jets.

2. A resonant manifold (length resonator) can be used to produce more total sound than can the pulse jet alone, and the frequency of the resonant combustion can also be markedly increased by the addition of a resonant manifold.

Phase II. Phase II progress is evidenced by the successful operation of the PJ-RMS at pressures as high as 350 kPa. No operational difficulties were caused by these increased pressures. There is reason to believe that the increased fuel/air mass flow rates associated with increased operating pressure resulted in increased sound levels. Although operation of the pulse jet at 810 to 1015 kPa (the objective of the Phase II effort) is yet to be demonstrated, there is no reason to doubt that this can be achieved. Operation of the pulse jet at pressures significantly above atmospheric pressure constitutes another significant advance in pulse-jet technology.

Conclusions. On the basis of the developmental work at the University of Toronto, the feasibility of PJ-ADC for PFBC application continues to look technically feasible. The uncertainty regarding the feasibility of PJ operation at elevated pressures appears to be all but removed. Although the developmental work necessary to extend the operating characteristics of previously existing pulse-jet designs has been significantly greater than anticipated, continued examination of PJ-ADC for high-temperature/high-pressure applications such as PFBC is warranted.

b. High-Efficiency Cyclone

A Donaldson Co. TAN-JET cyclone, claimed to have better dust-removal efficiency than conventional cyclones, has been installed in the flue-gas system of the ANL 15.2-cm-dia combustor for testing and evaluation. The cyclone will also be used in testing of the ANL granular-bed filter concept and in testing of a pulse jet-acoustic dust conditioning system for enhanced particle removal.

The TAN-JET employs a secondary flow of clean air to improve gas-solid separation in the primary air flow of dirty gas entering the cyclone. The secondary air flow is preheated to the temperature of the incoming primary gas and enters the cyclone through a nozzle centrally located in the cyclone barrel.

Tests at Ambient Conditions. A series of experiments have been performed at ambient conditions (no combustion, fluidized bed of limestone in the combustor) as a preliminary step to evaluation of the cyclone. Figure 6 illustrates the present arrangement of the PDU combustion test system, with the TAN-JET cyclone currently functioning as the secondary cyclone.

For these preliminary experiments, the combustion system was pressurized to about 250 kPa. A bed of fresh limestone in the combustor was fluidized at a superficial gas velocity of about 0.76 m/s, generating a dust-laden gas. Fresh limestone was continually fed to the combustor, and a constant bed level was maintained via a 0.91-m high overflow standpipe.

After steady operation during an experiment was established, the primary cyclone and TAN-JET cyclone hoppers were emptied and a timed period of solids collection was initiated. During this period, the flue gas downstream from the TAN-JET cyclone was sampled at the sampling port location (see Fig. 6) using an Andersen cascade impactor. The efficiencies of the primary and

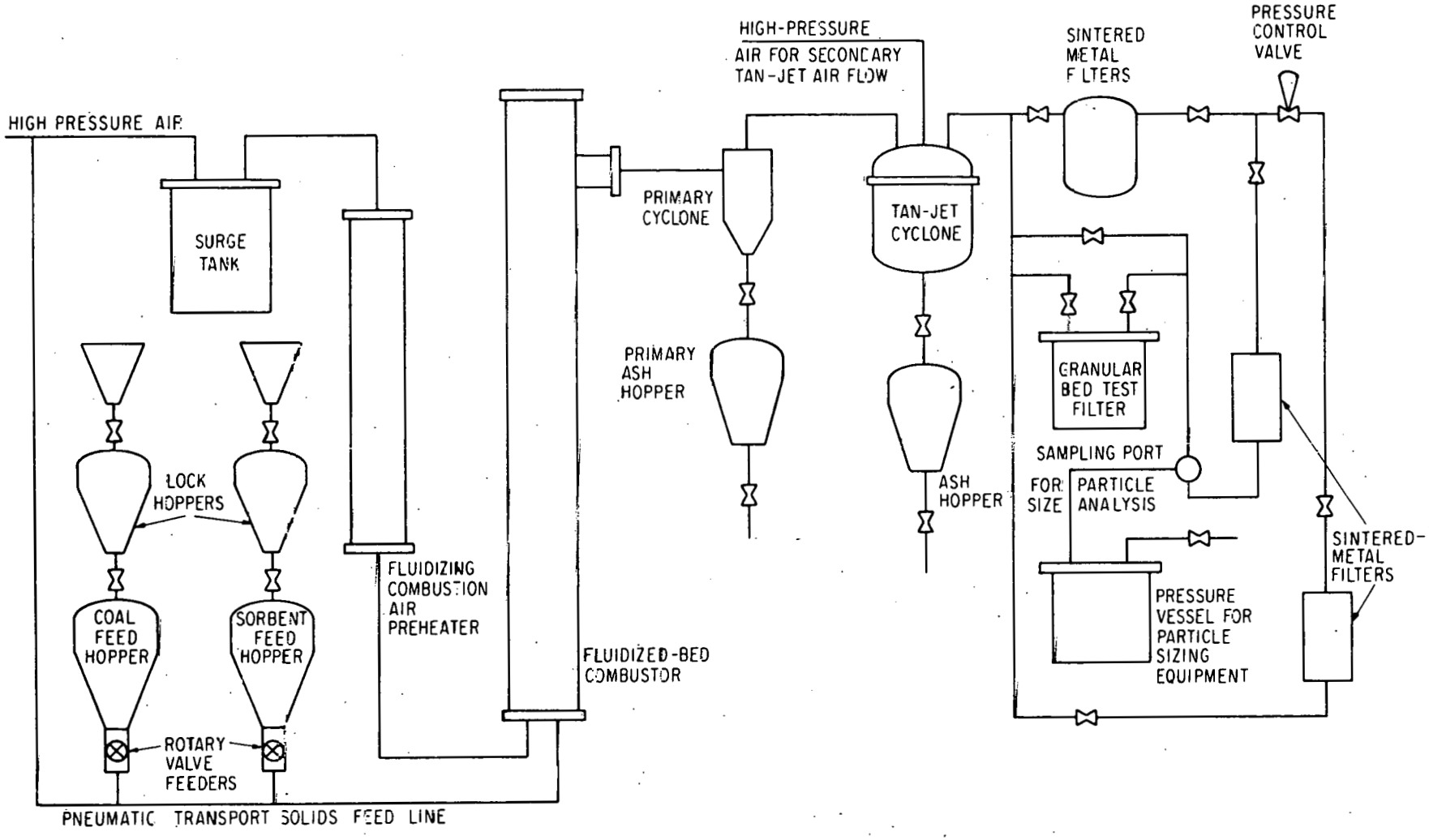


Fig. 6. Schematic Flow Sheet of PFBC System

Table 7. Preliminary Experiments in the Evaluation of TAN-JET Cyclone

| ΔP Across TAN-JET Nozzle, kPa | Expt. No. | Exit-Gas Particle Loading | | | Particle Collection Efficiency | | |
|---|---|---|---|---|---|---|---|
| | | Combustor, $g/m^3$ | Primary Cyclone, $g/m^3$ | TAN-JET Cyclone, $g/m^3$[a] | Primary Cyclone, % | TAN-JET Cyclone, % | Combined, % |
| ~70 | 2 | 12 | 0.62 | 0.11 | 95 | 81 | 99.0 |
| | 6 | 17 | 1.1 | 0.17 | 94 | 82 | 98.9 |
| | 8 | 31 | 1.5 | 0.14 | 95 | 90 | 99.5 |
| ~100 | 1 | 5.0 | 0.29 | 0.08 | 94 | 69 | 98.1 |
| | 5 | 25 | 1.4 | 0.12 | 95 | 90 | 99.5 |
| | 9 | 13 | 0.69 | 0.13 | 95 | 79 | 99.0 |
| ~140 | 3 | 2.3 | 0.34 | 0.08 | 86 | 74 | 96.4 |
| | 7 | 18 | 1.5 | 0.12 | 92 | 90 | 99.2 |
| | 10 | 12 | 1.2 | 0.14 | 90 | 86 | 98.6 |

[a]Total air (main air flow plus secondary air)

TAN-JET cyclones were then calculated from the amounts of solids collected in their respective ash hoppers and from the solids loading downstream from the TAN-JET as determined with the cascade impactor.

The results of the experiments are summarized in Table 7. Three experiments were performed at each of three levels of pressure drop (about 70, about 100, and about 140 kPa) across the TAN-JET secondary air inlet nozzle. At 70, 100, and 140 kPa pressure drop across the nozzle, the secondary air flows represented about 10, about 12, and about 23% of the total gas flow (primary plus secondary) through the TAN-JET cyclone, respectively.

Solids loadings in the flue gas leaving the TAN-JET cyclone ranged from 0.08 to 0.17 $g/m^3$. Collection efficiency ranged from 69 to 90%.

In Fig. 7, the collection efficiency data is presented as percent penetration (100% - collection efficiency) as a function of the mass loading entering the TAN-JET cyclone. As expected, percent penetration decreased with increases in mass loading to the cyclone. At an inlet mass loading of about 0.3 $g/m^3$, penetration was measured to be about 30%. At an inlet mass loading of about 1.5 $g/m^3$, penetration was measured to be only about 10%. The tests were not sufficiently sensitive, however, to assess the effect of the nozzle pressure drop on the collection efficiency. Penetration at a given inlet mass loading would be expected to decrease with increasing nozzle pressure drop.

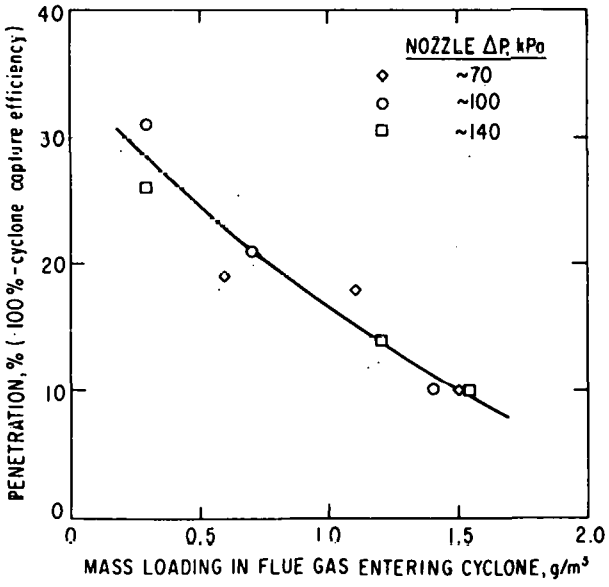


Fig. 7. Penetration of Flue Gas Particulate Matter Through TAN-JET Cyclone as a Function of Mass Loading in Flue Gas Entering the Cyclone.

Figure 8 is a plot of the mass loading in the flue gas leaving the TAN-JET as a function of the mass loading in the gas entering the cyclone. Although this data exhibits scatter, it does indicate (as expected) that the above-discussed increases in cyclone efficiency with increases in inlet mass loading are insufficient to prevent the outlet mass loading from increasing at higher inlet mass loadings.

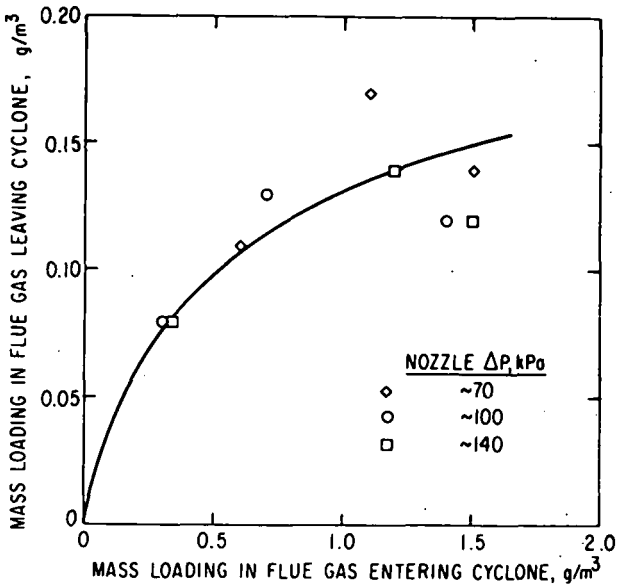


Fig. 8 Mass Loading in Flue Gas Leaving TAN-JET Cyclone as a Function of Mass Loading in the Flue Gas Entering Cyclone.

Tests during Combustion Experiments. Several experiments have been completed to test and evaluate the TAN-JET cyclone during combustion experiments in the PDU. Conditions in the combustor were: (1) Sewickley coal, (2) Greer limestone sorbent, (3) 855°C combustion temperature, (4) 304-kPa operating pressure, and (5) approximately 17% excess combustion air.

Results of the tests completed are given in Table 8. As compared with the experiments at ambient conditions, in combustion experiments the loadings leaving the primary cyclone and entering the TAN-JET were considerably higher. In these experiments, loadings to the TAN-JET ranged from about 2.2 $g/m^3$ to about 3.4 $g/m^3$. The loadings in the preliminary experiments ranged from about 0.3 $g/m^3$ to about 1.5 $g/m^3$. At the high inlet loadings, the TAN-JET collection efficiency ranged from about 91% to about 95% and loadings in the outlet gas from the TAN-JET ranged from about 0.15 to 0.24 $g/m^3$.

The data are also presented in Figs. 9 and 10. (The open symbols are the ambient temperature data also presented in Figs. 7 and 8). The solid symbols represent the data obtained during combustion experiments. Figure 9 illustrates the penetration of particles through the TAN-JET cyclone as a function of the mass loading in the flue gas entering the cyclone. Figure 10 illustrates the mass loading in the flue gas leaving the TAN-JET cyclone, also as a function of inlet mass loading.

As can be seen from Fig. 9, the penetration data obtained in combustion experiments is consistent with the penetration data obtained under lower loading conditions in the ambient experiments. Penetration continues to decrease with an increase in inlet mass loading.

Table 8. TAN-JET Collection Efficiency in Combustion Experiments

| ΔP Across TAN-JET Nozzle, kPa | Expt. No. | Exit-Gas Particle Loading | | | Particle Collection Efficiency | | |
|---|---|---|---|---|---|---|---|
| | | Combustor, $g/m^3$ | Primary Cyclone, $g/m^3$ | TAN-JET Cyclone, $g/m^3$[a] | Primary Cyclone, % | TAN-JET Cyclone, % | Combined, % |
| 100 | 8001LP1B | 35.1 | 3.15 | 0.151 | 90.1 | 95.2 | 99.1 |
| 100 | 8001LP1D | 37.7 | 3.18 | 0.148 | 90.8 | 95.2 | 99.2 |
| 100 | 8001LP1D | 35.2 | 2.54 | 0.147 | 91.7 | 94.4 | 99.2 |
| 70 | 8001LP1E | 30.3 | 2.16 | 0.196 | 91.8 | 90.9 | 98.9 |
| 70 | 8001LP1E | 28.7 | 3.39 | 0.243 | 86.8 | 92.8 | 98.6 |
| 140 | 8001LP1F | 31.4 | 3.24 | 0.148 | 88.7 | 95.4 | 99.0 |

[a]Total air (main air flow plus secondary air)

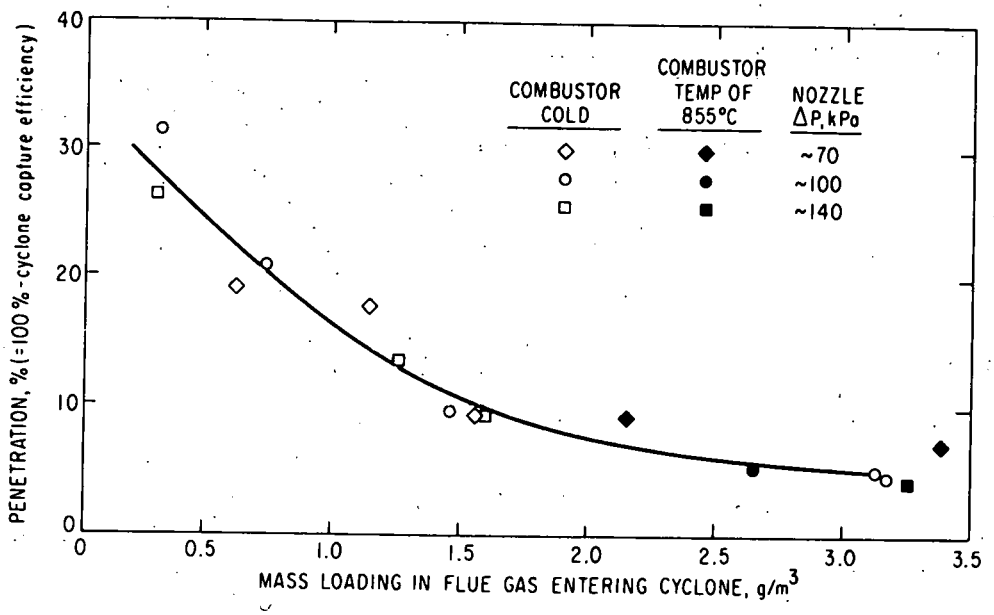


Fig. 9. Penetration vs. Mass Loading in Flue Gas Entering TAN-JET Cyclone

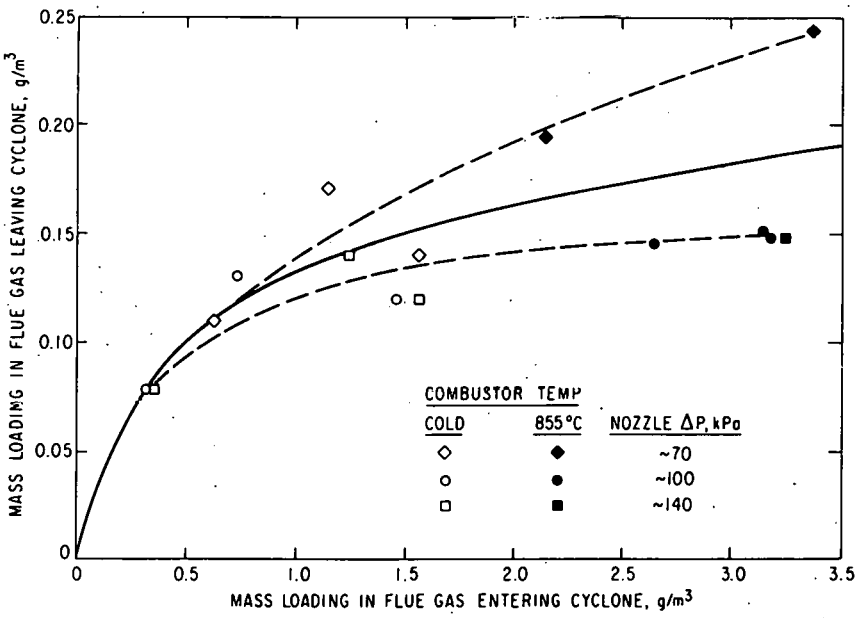


Fig. 10. Mass Loading Leaving TAN-JET Cyclone vs. Mass Loading Entering Cyclone

The effect on cyclone efficiency of the pressure drop of the secondary air flow nozzle, which was not readily apparent from the ambient data, is illustrated in Fig. 10. In the high range of inlet mass loading, 2.0 to 3.5 $g/m^3$, particulate removal was significantly worse at about 70 kPa pressure drop than at greater pressure drops. At the higher (about 100 and about 140 kPa) pressure drops, performance was independent of pressure drop. In fact, at the higher pressure drops, very little increase in outlet mass loading was observed as the inlet mass loading increased from about 1 to over 3 $g/m^3$.

The results illustrated in Fig. 10 are encouraging. At nozzle pressure drops greater than 100 kPa, the mass loading in the flue gas leaving the cyclone was less than 0.15 $g/m^3$, even for inlet mass loadings as high as 3.2 $g/m^3$.

Additional experiments are planned to operate the system at higher pressure (about 810 kPa) and to generate information on separation efficiency as a function of particle size.

## TASK C. LIMESTONE UTILIZATION

### 1. Enhancement of Limestone Sulfation
(J. A. Shearer and C. B. Turner)

Extensive work has been done in this laboratory on characterizing the effects of inorganic salts on limestone sulfation.[15] Results have shown that for all limestones investigated, maximum sulfation is achieved when the average pore diameter of the calcined material is near 0.3 μm. Previous work on limestone sulfation demonstrated that pores larger than 0.3 μm appear to be most important in reactions with $SO_2/O_2$ mixtures.[16] In this work, surface areas as well as porosities have been measured for the untreated limestones investigated. Table 9 lists total surface areas, surface areas of pores $\geq$0.3 μm, total pore volumes, and pore volumes of pores $\geq$0.3 μm for limestones calcined 1 h in 5% $O_2$, 20% $CO_2$, and the balance $N_2$. The stones are listed in the order of their increasing $CaCO_3$ content (indicated by the first two digits of their number designations).

No correlation of either surface area or pore volume with $CaCO_3$ content is apparent. The porosity of the calcined stones reflects the original porosity of the natural limestones, as well as the effects of impurities on the resultant porosity of the calcined material.

As mentioned earlier, literature data[16] on the reactivity of calcium carbonate-containing rocks with $SO_2$ indicated that porosity and reactivity are related. Data collected during this investigation on sulfation reactivity of limestones exposed to a simulated flue gas at 850°C are plotted against total pore surface area (Fig. 11) rather than porosity or pore volume. There is no correlation of reactivity with total porosity. However, there is an obvious relationship (Fig. 12) of the percent conversion to sulfate and the surface area of pores $\geq$0.3 μm in diameter (as measured with a mercury porosimeter). The data indicate that as the surface area of pores larger than 0.3 μm diameter increases, sulfation of the lime increases, leveling off at 50-60% conversion (the apparent maximum range of sulfation for pure limestones).

When these limestones are treated with either NaCl or $CaCl_2$, their surface areas change greatly. At low levels of salt addition, pore surface area increases, but with greater salt additions and subsequent enlargement of pores and loss of micropores, pore surface area decreases. Figure 13 shows conversion versus surface area of pores $\geq$0.3 μm for (1) untreated stones (also given in Fig. 12) and (2) salt-treated stones having a wide variety of reactivities. Conversion for all treated stones approaches 50%, a conversion exhibited by only the most reactive of untreated limestones.

Table 9. Pore Volumes and Surface Areas for 18-20 mesh Limestones[a] Calcined 1 h in 20% $CO_2$, 5% $O_2$, and the balance $N_2$ at 850°C

| Stone | Total Surface Area, $cm^2/g$ | Surface Area for Pores $\geq$0.3 μm, $cm^2/g$ | Total Pore Volume, $cm^3/g$ | Pore Volume for Pores $\geq$0.3 μm, $cm^3/g$ |
|---|---|---|---|---|
| ANL-6702 | 87,742 | 12,510 | 0.423 | 0.219 |
| ANL-7401 | 89,795 | 6,764 | 0.423 | 0.130 |
| ANL-8001 | 58,114 | 8,868 | 0.325 | 0.118 |
| ANL-8101 | 129,121 | 3.612 | 0.453 | 0.175 |
| ANL-8301 | 163,603 | 2,108 | 0.403 | 0.058 |
| ANL-8701 | 68,297 | 14,537 | 0.396 | 0.161 |
| ANL-8901 | 109,217 | 6,253 | 0.357 | 0.109 |
| ANL-8902 | 92,397 | 3,236 | 0.310 | 0.055 |
| ANL-8903 | 91,923 | 6,478 | 0.369 | 0.107 |
| ANL-9201 | 134,793 | 1,315 | 0.325 | 0.080 |
| ANL-9401 | 87,146 | 29,066 | 0.508 | 0.280 |
| ANL-9402 | 124,779 | 1,370 | 0.277 | 0.050 |
| ANL-9501 | 188,442 | 877 | 0.375 | 0.051 |
| ANL-9502 | 73,057 | 12,770 | 0.382 | 0.156 |
| ANL-9503 | 113,907 | 9,227 | 0.512 | 0.243 |
| ANL-9504 | 112,596 | 2,981 | 0.351 | 0.055 |
| ANL-9505 | 80,099 | 4,660 | 0.338 | 0.130 |
| ANL-9601 | 197,599 | 2,099 | 0.454 | 0.160 |
| ANL-9602 | 116,824 | 4,251 | 0.345 | 0.092 |
| ANL-9603 | 90,043 | 3,297 | 0.295 | 0.070 |
| ANL-9701 | 120,202 | 2,090 | 0.351 | 0.051 |
| ANL-9702 | 175,777 | 2,285 | 0.353 | 0.090 |
| ANL-9703 | 108,540 | 9,736 | 0.519 | 0.281 |
| ANL-9704 | 82,474 | 8,378 | 0.388 | 0.120 |
| ANL-9801 | 113,486 | 4,393 | 0.430 | 0.144 |
| ANL-9802 | 93,698 | 6,727 | 0.488 | 0.260 |
| ANL-9901 | 110,056 | 6,187 | 0.392 | 0.116 |
| ANL-9902 | 100,952 | 9,655 | 0.473 | 0.214 |
| Calcite | 285,350 | 619 | 0.281 | 0.038 |

[a]Stone compositions are given in Reference 15.

Pore volumes (determined directly from mercury porosimetry measurements) are related to surface areas of limes. Whereas Fig. 14 shows a weak correlation between total pore volume and conversion to sulfate of the available CaO, the correlation with sulfation reactivity is greatly improved by considering only the volume of pores with diameters larger than 0.3 μm (Fig.15). This correlation allows the reactivity of a given limestone with $SO_2/O_2$ to be roughly predicted relative to other limestones being considered. This has application to fluidized-bed coal combustion where the choice of limestone is limited more by geographic location of limestone formation than any other factor.

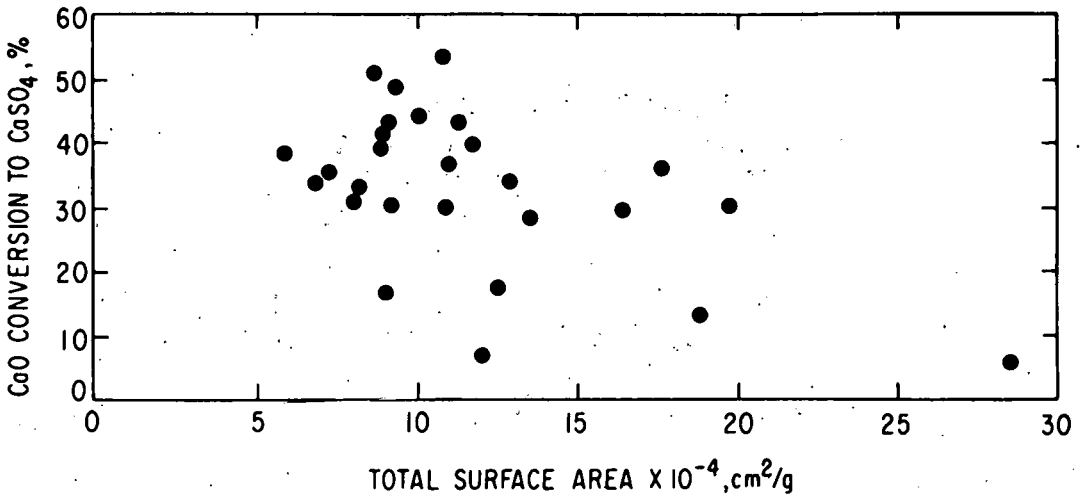


Fig. 11. Sulfation vs. Total Surface Area for 18-20 Mesh Limestone Sulfated at 850°C for 6 h in 0.3% $SO_2$, 5% $O_2$, 20% $CO_2$ and the balance $N_2$

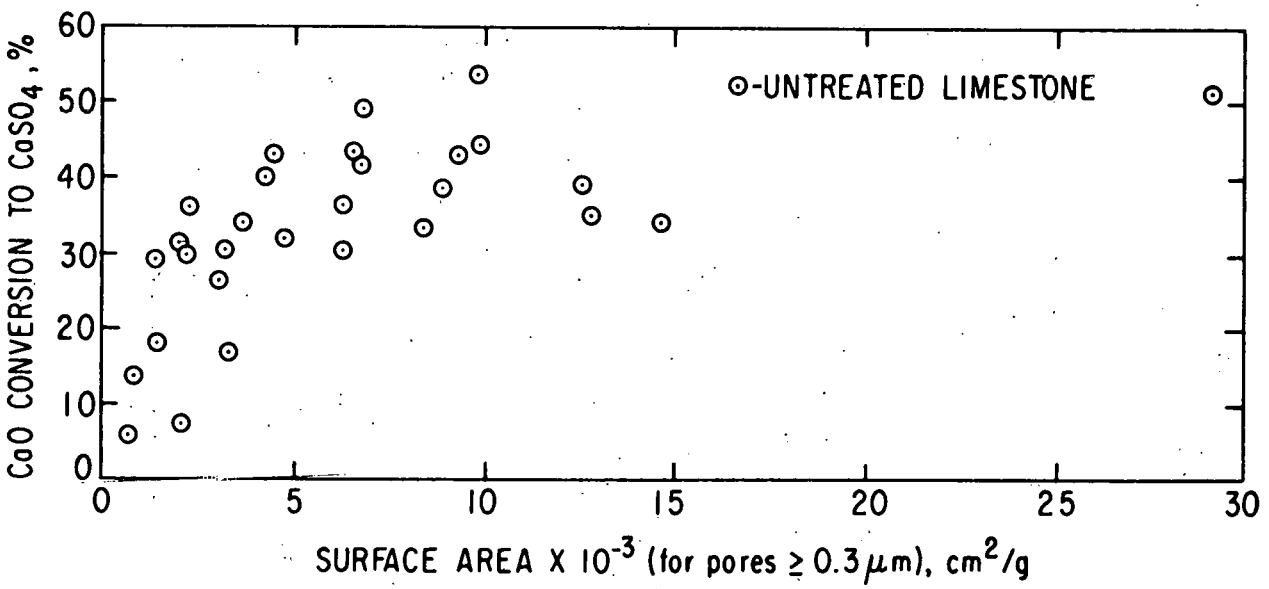


Fig. 12. Percent Sulfation vs. Surface Area of Pores >0.3 μm in Untreated 18-20 Mesh Limestones Sulfated at 850°C for 6 h in 0.3% $SO_2$, 5% $O_2$, 20% $CO_2$, and the balance $N_2$

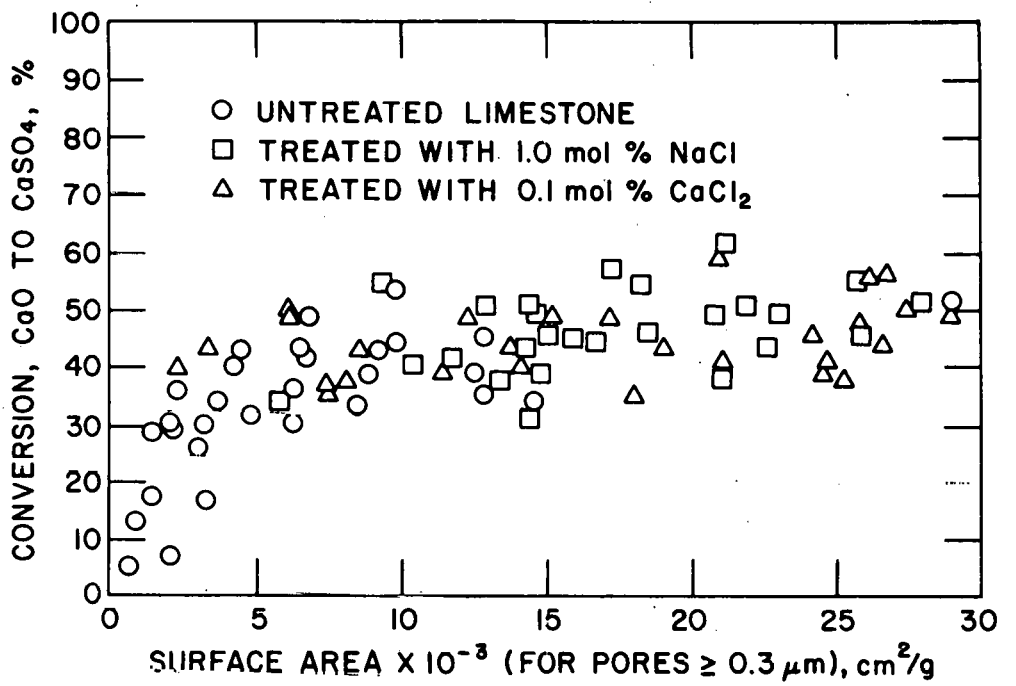


Fig. 13. Percent Sulfation vs. Surface Area of Pores ≥0.3 μm for Untreated 18-20 Mesh Limestone and Limestones Treated with NaCl and $CaCl_2$. Sulfation at 850°C for 6 h in 0.3% $SO_2$, 5% $O_2$, 20% $CO_2$, and the balance $N_2$

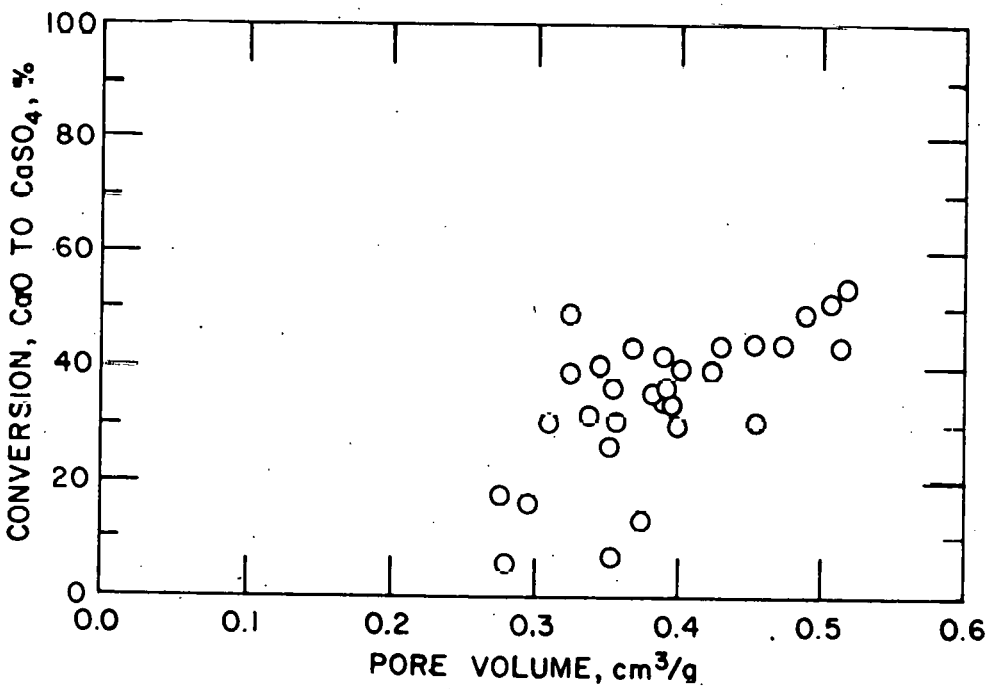


Fig. 14. Sulfation vs. Total Pore Volume in Limestones. Sulfation at 850°C for 6 h in 3% $SO_2$, 5% $O^2$, 20% $CO_2$ and the balance $N_2$

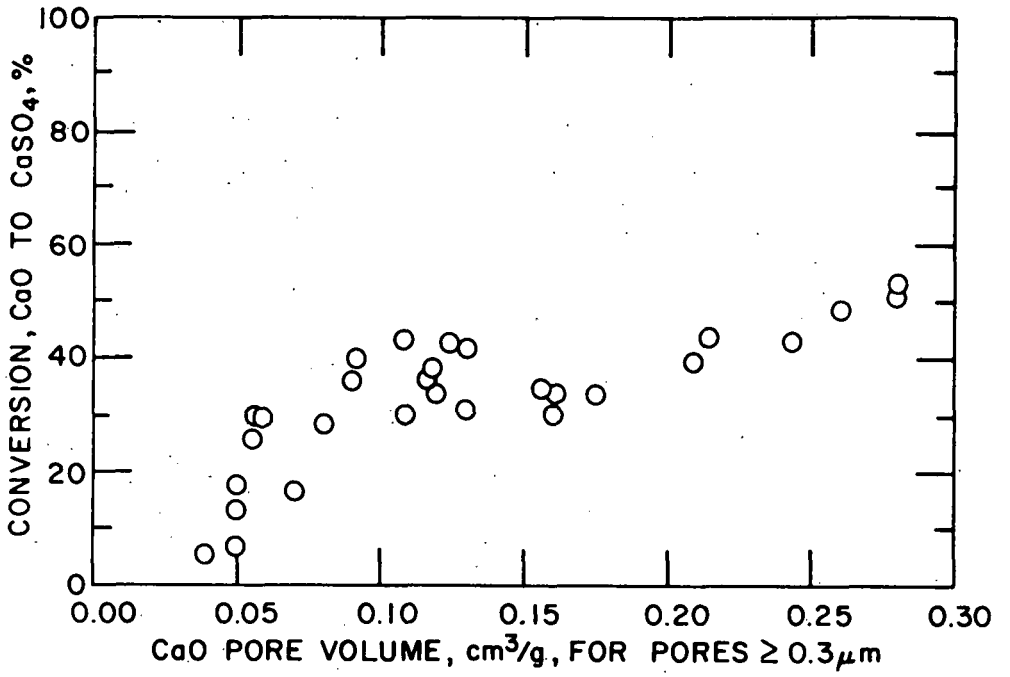


Fig. 15. Sulfation vs. Pore Volume for 18-20 Mesh Limestones Sulfated at 850°C for 6 h in 0.3% $SO_2$, 5% $O_2$, 20% $CO_2$ and the balance $N_2$

At present, investigation of the effects of $CaCl_2$ on dolomites and the sulfating capacities of the $CaCl_2$-treated calcines is being completed. Scanning electron microphotographs are being prepared to provide visible evidence of $CaCl_2$ effects on both limestones and dolomites.

When amounts of salts greater than 1 mol % are added, surface area and reactivity decrease under laboratory conditions. Conversion of CaO to $CaSO_4$ appears to be related to the surface area for pores $\geq$0.3 μm. Larger surface areas produce maximum reactivity which is limited by the structural space requirements of the large $CaSO_4$ molecule.

Investigation of the effects of additives during sulfation of limestones has shown major effects on the physical structure of the stones. Scanning electron microscopy has been successfully used in conjunction with mercury porosimeter data to describe in detail the changes that occur during calcination and sulfation of treated limestones (see below).

The use of NaCl as a sulfation-enhancer has received most of the experimental attention.[15] A suggested mechanism proposes that trace amounts of liquid phase form, lowering the activation energy of decomposition and recrystallization and thereby accelerating the ionic rearrangement and increasing porosity in the lime.

It was uncertain whether a liquid or vapor phase forms. The structures seen in the photographs in Fig. 16 provide a partial answer. Figure 16 shows two views of a calcite spar crystal treated with a minute amount of NaCl. The salt crystallized from an aqueous solution as discrete particles during treatment. Upon heating of the particles at 850°C for 40 min, a liquid formed which interacted in a gradually enlarging sphere around the point of contact with the calcite crystal. Lessening structural changes in circles around salt particles strongly suggest a liquid phase interaction. The presence of a vapor phase would have produced a more uniform attack over the entire sample.

In this investigation, the effects of $CaCl_2$ on limestone sulfation were also studied (ANL/CEN/FE-78-3). The mechanism of interaction of limestone containing small concentrations of this salt was suggested to be similar to that with NaCl. Figure 17 illustrates the effects of various amounts of $CaCl_2$ upon the calcination of ANL-9501 limestone. Also illustrated are two untreated samples that were calcined for different lengths of time.

Firing for a long duration has the effect of increasing the porosity as indicated by Fig. 17b; this photograph shows uniform pores over the entire particle. These pores are larger than those produced by 2-h firing (Fig. 17a).

In sharp contrast to NaCl, small amounts of $CaCl_2$ have a large effect. Extensive pore growth and crystallite clumping occurred (Fig. 18) similar to the effects produced by large amounts of NaCl, (shown in photographs presented earlier).[15] As the concentration of $CaCl_2$ increased, the extent of crystal growth increased, and pore size gradually increased. At levels of salt addition greater than 1 mol % $CaCl_2$, the lime particles begin to fuse together (Fig. 18). At this point, large amounts of liquid phase formed that were capable of dissolving CaO in substantial amounts, as shown by the phase diagram for this system.[17] Figure 18 illustrates this characteristic flow structure in ANL-9501 limestone. Figures 18b and 18c show the junction of two separate limestone particles at two magnifications. The point of contact is between the darker image and the lighter image. The particles have fused together yet retain some coarse porosity. At the sulfation temperature, this is a very fluid system containing dissolved CaO and hence has great potential to react with $SO_2/O_2$ mixtures. The extent of reaction is limited only by the presence of sufficient liquid phase to dissolve residual unreacted CaO.

Sulfation experiments show that indeed there is maximum sulfation (50% conversion) at low salt concentrations; conversion starts to decrease when these low $CaCl_2$ additions are exceeded. At $CaCl_2$ concentrations above 1.0 mol %, however, the extent of sulfation begins to increase rapidly; with continued $CaCl_2$ addition, conversion approaches 100%. Practical application of this information is limited since the high salt concentrations produce sticky particles that may cause problems in maintaining fluidization in a fluid-bed combustor. However, $CaCl_2$ has been successfully added to injected limestone powder in a large-scale fixed-bed combustor to enhance the sulfation, removing sulfur from exhaust gases at very high temperatures (>1000°C).[18]

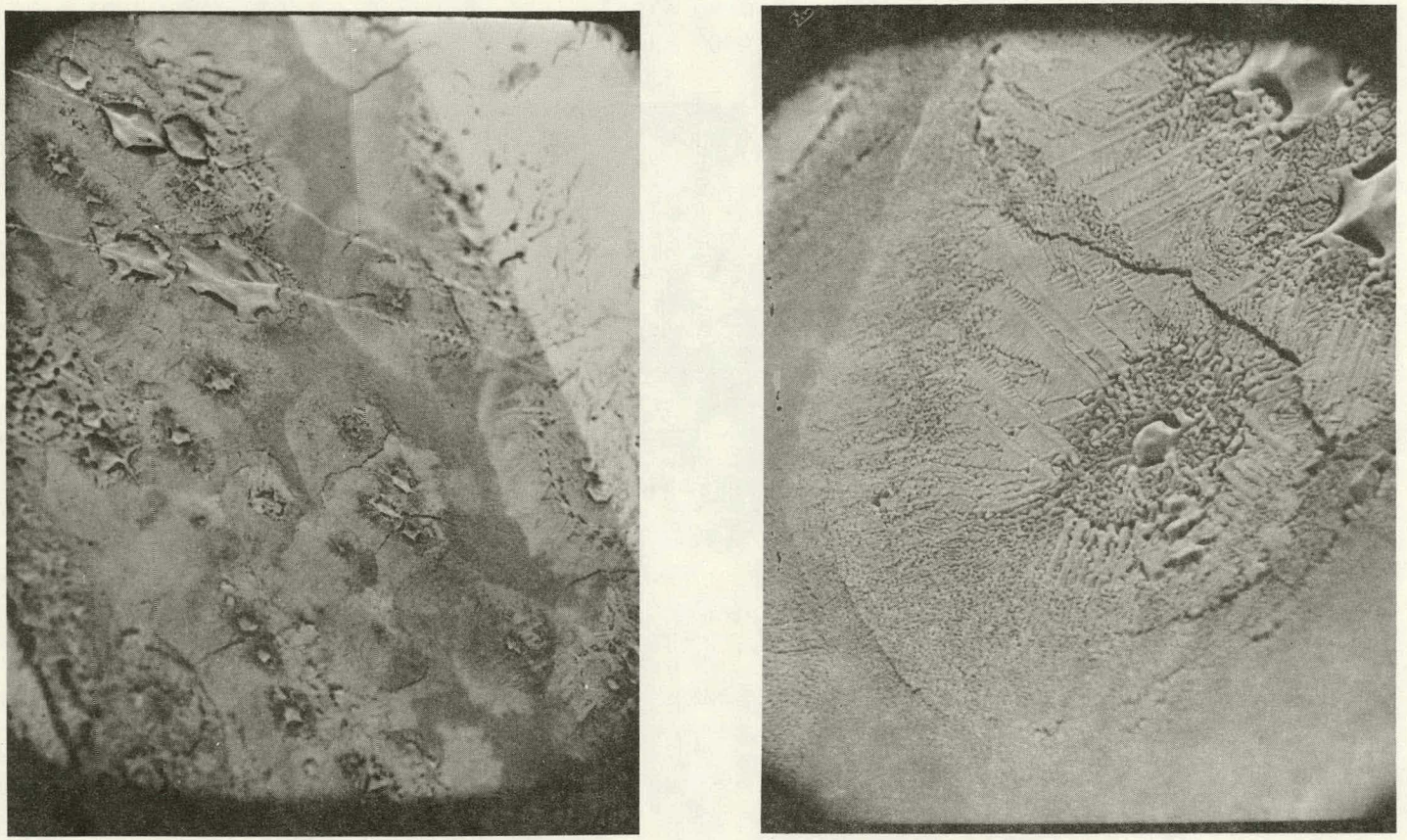

a
(260X)

b
(1300X)

Fig. 16. Surface of Calcite Spar Particle (two views) Calcined with 0.2 wt % NaCl in 20% $CO_2$, 5% $O_2$, and the balance $N_2$ at 850°C for 40 min. ANL Neg. No. 308-78-418.

a. 9501 Calcined 2 h (700X)

b. 9501 Calcined 6 h (700X)

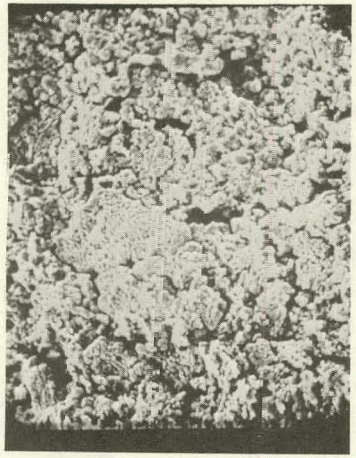

c. 9501 + 0.1 mol % $CaCl_2$ Calcined 1 h (700X)

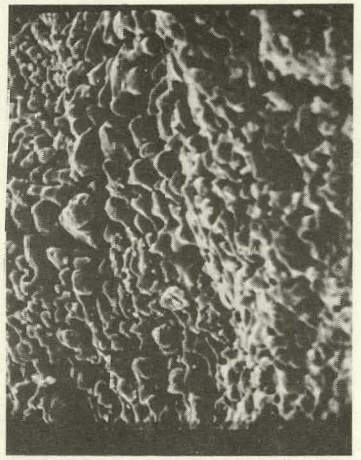

d. 9501 + 0.5 mol % $CaCl_2$ Calcined 1 h (650X)

e. 9501 + 1.0 mol % $CaCl_2$ Calcined 1 h (675X)

Fig. 17. Limestone ANL-9501 Particle Cross Sections. Various calcination treatments at 850°C in %5 $O_2$, 20% $CO_2$, and the balance $N_2$. ANL Neg. No. 308-78-420

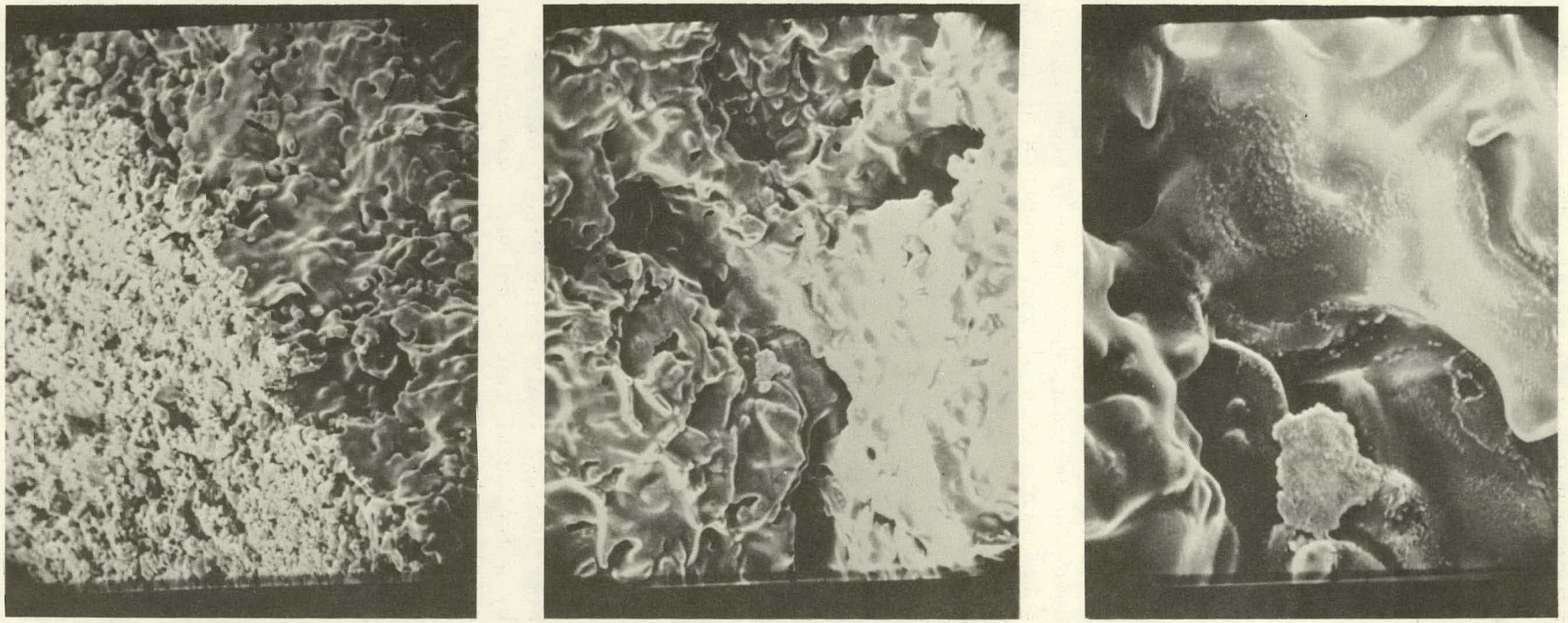

a.

9501 + 1.0 mol % $CaCl_2$
(520X)

b.

9501 + 2.0% $CaCl_2$
Junction of Two Particles
(520X)

c.

9501 + 2.0% $CaCl_2$
Jumction of Two Particles
(1920X)

Fig. 18. Limestone ANL-9501 with $CaCl_2$. Calcined 1 h at 850°C in 50% $O_2$, 20% $CO_2$, and the balance $N_2$. ANL Neg. No. 308-78-419

Extrapolation of laboratory tube furnace results to actual fluidized-bed combustor conditions would introduce many variables not present under controlled laboratory conditions.

Differences between limestones are currently being investigated with a polarizing microscope in order to relate structural properties to sulfur reactivities. Also, experiments are being initiated to examine the effects of reducing conditions on limestone reactivity and also on the effectiveness of inorganic sulfation enhancers. Products generated by a 15-cm-dia (6-in.-dia) combustor are also being characterized for comparison with laboratory samples that had been reacted in flow-through horizontal-tube furnaces. Attempts to isolate various reaction conditions to determine their effects on limestone sulfation are being pursued using both the laboratory-scale apparatus and the larger fluidized-bed combustors.

The effects on sulfation of the structure of calcined material (i.e., grain size and other properties determinable from SEM photographs) will be determined. In this report in the section, Petrographic Examination of Limestones, a polarizing microscopy evaluation of the structure of raw untreated stones is described.

## 2. Petrographic Examination of Limestones
(W. I. Wilson and J. A. Shearer)

Petrographic analyses of several calcareous rocks were made and compared with their limestone $SO_2$ reactivities to determine the basic structural reasons for wide variations in calcium utilization for carbonate rocks which have essentially the same chemical composition. The calcareous rocks studied have $CaCO_3$ contents ranging from 95 to 100 wt % (Table 10). One limestone has a total calcium utilization of approximately 20%. Four have total calcium utilizations ranging from approximately 31 to 38%, and three have total calcium utilizations ranging from approximately 52 to 66%.

Following vacuum-impregnation with epoxy resin of particles from each of the eight rocks, polished sections were made. These sections were examined in reflected polarized light. Average grain sizes were estimated. (These estimates may be in error by a factor of two to three.) To obtain an estimate, the predominant size of the grains present in the sample was determined with the microscope, and these values were assigned to one of three size categories: (1) fine, 4 to 63 μm across; (2) medium, 63 to 250 μm across, and (3) coarse, 250 μm across. More quantitative grain size measurement will be made by point-counting several hundred grains in thin sections of each sample (to be prepared later).

### a. ANL-9802*

Because the finer grains in this stone tend to pluck out during polishing, it is difficult to estimate the average grain size from the polished section of this limestone. Crushed particles viewed in transmitted light show that the average size is 3 to 6 μm. Normally, the vacuum impregnation treatment promotes greater retention of grains unless the permeability to epoxy is very low. The high reactivity of this limestone is probably linked with its high porosity, yet is limited somewhat by its apparently low gaseous permeability.

*Examined by L. H. Fuchs, Chemistry Division

b. ANL-9801 Limestone

This coarse-grained calcitic limestone is gray and contains a few dark gray seams which are probably carbonaceous stylolites. This limestone appears to be an equigranular rock (grains are all approximately the same size). The low reactivity of this stone is probably linked with its coarse granularity and its low porosity.

c. ANL-9703 Limestone

This stone appears to be a fine-grained porous carbonated limestone. The texture is somewhat loose, making it more highly reactive. The high reactivity of this stone is probably linked with its high porosity and fine grains.

d. ANL-9702 Limestone

This sample, more than any of the others, shows a distinct twinning characteristic (groups of two or more crystals in which the individuals grow together symmetrically so that they share a common plane). The grains vary greatly in size from medium to coarse. The coarse grains show the twinning characteristic of the limestone.

It is not certain what caused twin crystals in this limestone. However, the nature of this texture, as well as the stone porosity, may be significant in causing the low reactivity of the stone.

e. ANL-9701* (Germany Valley) Limestone

This limestone is fine grained and dense, but contains some coarser vein-deposited calcite. Grain sizes are predominantly near 5 μm. The fine-grained texture of this limestone is not conducive to higher reactivity. The densely packed crystallites probably indicate a low porosity.

f. ANL-9603 Limestone

The grain sizes of this limestone vary from fine to coarse. The coarse grains show a twinning characteristic similar to that of the ANL-9702 limestone sample. The total calcium utilization is also essentially the same as that of ANL-9702. Therefore, the nature of this texture, as well as its porosity, may be significant in determining the low reactivity of the stone.

g. ANL-9602 Limestone

The grains of this sample appear to have uniform sizes for the most part. They appear to be loosely packed crystallites, indicating high porosity and high permeability.

h. ANL-9501 (Grove) Limestone

This fine-grained limestone is uniformly gray and equigranular. The grains appear to be tightly interlocked. A few veinlets of calcite occur in some particles. The low reactivity of this stone probably results from its tightly interlocked grains.

---

* Examined by L. H. Fuchs, Chemistry Division

Table 10. Compositions of Limestones

| Limestone | $CaCO_3$, wt % | $MgCO_3$, wt % | $Fe_2O_3$, wt % | $Al_2O_3$, wt % | $SiO_2$, wt % | $Na_2O$, wt % | $K_2O$, wt % | TGA Total Ca Utilization, % |
|---|---|---|---|---|---|---|---|---|
| ANL-9802 | 98.2 | 0.47 | 0.18 | 0.10 | 0.29 | 0.04 | 0.01 | 61.8 |
| ANL-9801 | 98.3 | 0.6 | 0.15 | 0.16 | 0.20 | 0.04 | 0.20 | 35.3 |
| ANL-9703 | 97.6 | 0.58 | 0.19 | 0.50 | 1.08 | 0.03 | 0.17 | 66.2 |
| ANL-9702 (Germany Valley) | 97.5 | 0.68 | 0.05 | 0.05 | 0.21 | 0.01 | 0.01 | 31.0 |
| ANL-9701 | 97.8 | 0.6 | 0.10 | 1.8 | 0.2 | 0.25 | -- | 18.7 |
| ANL-9603 | 96.4 | 1.56 | 0.10 | 0.30 | 0.70 | 0.05 | 0.11 | 32.1 |
| ANL-9602 | 96.2 | 0.43 | 0.12 | 0.21 | 1.19 | 0.03 | 0.01 | 51.7 |
| ANL-9501 (Grove) | 95.3 | 1.3 | 0.09 | 0.25 | 0.77 | 0.03 | -- | 37.5 |

i. Conclusion

It remains uncertain whether the petrographic properties of the limestones account for their differences in reactivities. The data do not clearly indicate that petrographic texture influences $SO_2$ reactivity. Further work in which crystal defects such as intracrystalline or intragranular voids, fluid inclusions, and twin lamellae are studied may enable us to predict sulfur reactivity more accurately from petrographic data.

## REFERENCES


1. Stephen Brunauer, The Adsorption of Gases and Vapors, Vol. 1, Physical Adsorption, Princeton University Press, p. 13 (1945).

2. J. G. Vail, Soluble Silicates--Their Properties and Uses, 1st Ed., Reinhold Publishing Corporation, New York (1952).

3. R. K. Iler and E. J. Tauch, Sodium Silicate and Hydrochloric Acid from Sand, Salt and Steam, Trans. Am. Inst. Chem. Eng. 37, 853-877 (1941).

4. Kirk-Othmer Encyclopedia of Chemical Technology, 2nd Ed., Vol. 18, Interscience Publishers, New York, p. 134 (1963).

5. W. T. Reid, Ed., External Corrosion and Deposits--Boilers and Gas Turbines, 1st Ed., American Elsevier Publishing Comp., Inc., New York (1971).

6. W. Nelson and E. S. Lisle, High-Temperature External Corrosion on Coal-Fired Boilers: Siliceous Inhibitors, J. Inst. Fuel 38, 179-186 (1965).

7. W. M. Swift, S. H. D. Lee, J. C. Montagna, G. W. Smith, I. Johnson, G. J. Vogel, and A. A. Jonke, Plans and Studies on Flue Gas Cleaning and Particulate Monitoring in PFBC, presented at the 5th International Conference on Fluidized-Bed Combustion, Dec. 12-14, 1977, Washington, D.C., Part III.

8. S. K. Chirkov, The Preparation of Water Glass without the Use of Alkalies, J. Chem. Ind. (Moscow) 13, 469-474 (1939).

9. R. L. McCarron, A. M. Beltran, H. S. Spacil, and K. L. Luthra, Turbine Materials Corrosion in the Coal-Fired Combined Cycle, presented at the 5th International Conference on Fluidized-Bed Combustion Dec. 12-14, 1977, Washington, D. C.

10. D. L. Keairns et al., Fluidized Bed Combustion Process Evaluation, Environmental Protection Agency Report EPA-650/2-75-027-c (1975).

11. D. S. Scott, W. M. Swift, and G. J. Vogel, Pulse-Jet Acoustic Dust Conditioning in High-Temperature/Pressure Applications, Proc. EPA/ERDA Symp. on HIgh-Temperature/Pressure Particulate Control, Washington, D.C. (September 1977).

12. D. S. Scott, J. Sound Vib. 43, 607 (1975).

13. R. Razgaitis, An Analysis of the High-Temperature Particulate Collection Problem, Argonne National Laboratory Report ANL-77-14 (1977).

REFERENCES (contd)

14. C. K. Groves, The Development of a Pulse-Jet Driven Acoustical Dust Conditioner for High Temperature/Pressure Application, B.A. Sc. thesis, Division of Eng. Sci., Faculty of Appl. Sci. and Engr., Univ. of Toronto (March 1978).

15. J. A. Shearer, I. Johnson, and C. B. Turner, The Effect of Sodium Chloride on the Reaction of $SO_2/O_2$ Mixtures with Limestones and Dolomites, Argonne National Laboratory Report ANL/CEN/FE-78-8.

16. R. H. Borgwardt and R. Harvey, Environ. Sci. Technol. 6, 350 (1972).

17. D. A. Wenz, I. Johnson, and R. D. Wolson, J. Chem. Eng. Data 14, 250 (1969).

18. Private communication (1978).

Distribution for ANL/CEN/FE-79-3

Internal:

L. Burris
W. L. Buck
F. Cafasso
E. Carls
P. T. Cunningham
J. Fischer
H. Huang
B. R. Hubble
I. Johnson (20)
A. A. Jonke (30)
J. A. Kyger
R. V. Lancy
S. Lawroski
S. H. Lee
J. F. Lenc
W. A. Ellingson
L. Cuba
G. M. Kesser
E. G. Pewitt
F. F. Nunes
W. Podolski
J. Royal
S. Siegel
J. W. Simmons
G. W. Smith
R. B. Snyder
W. M. Swift
F. G. Teats
S. Vogler
R. G. Matlock
D. S. Moulton
D. S. Webster
W. I. Wilson
J. E. Young
R. Bane
E. J. Croke
J. D. Gabor
K. Jensen
N. Sather
J. Shearer
E. Smyk
C. B. Turner
A. B. Krisciunas
ANL Contract File
ANL Libraries (5)
TIS Files (6)

External:

DOE-TIC, for distribution per UC-90e (270)
Manager, Chicago Operations and Regional Office, DOE
Chief, Office of Patent Counsel, DOE-CORO
V. H. Hummel, DOE-CORO
President, Argonne Universities Association
Chemical Engineering Division Review Committee:
- C. B. Alcock, U. Toronto
- R. C. Axtmann, Princeton Univ.
- R. E. Balzhiser, Electric Power Research Institute
- J. T. Banchero, Univ. Notre Dame
- T. Cole, Ford Motor Co.
- P. W. Gilles, Univ. Kansas
- R. I. Newman, Allied Chemical Corp.
- G. M. Rosenblatt, Pennsylvania State Univ.

S. Saxena, Univ. Illinois, Chicago
D. H. Archer, Westinghouse Research Labs.
E. C. Bailey, John Dolio and Associates
S. Beall, Oak Ridge National Laboratory
O. L. Bennett, West Virginia U.
R. Bertrand, Exxon Research and Engineering (5)
M. Boyle, Valley Forge Labs.
J. A. Brooks, Amoco Oil Co.
R. D. Brooks, General Electric Co.
C. Busch, Spectron Development Laboratory, Inc.
J. Chen, Lehigh U.
D. Cherrington, Exxon Research and Engineering Co., Florham Park, NJ
J. Clark, Tennessee Valley Authority
D. Clarke, Stearns-Rogers
N. Coates, The MITRE Corporation
R. C. Corey, DOE-CCU
R. Covell, Combustion Engineering, Inc.

G. Curran, Conoco Coal Development Co.
D. DeCoursin, Fluidyne Engineering Co.
J. Dodge, Tetra Tech, Inc.
M. Dudukovic, Washington U.
S. Ehrlich, Electric Power Research Institute
M. Evans, Aerotherm Division of ACUREX Corporation
M. H. Farmer, Exxon Research & Engineering Co., Linden, NJ
C. Fisher, Univ. Tennessee
T. Fitzgerald, Oregon State U.
J. F. Flagg, Universal Oil Products Co.
H. B. Forbes, Stone & Webster Engineering Corp.
R. L. Gamble, Foster Wheeler Energy Corporation
D. E. Garrett, Garrett Energy Research and Engineering, Inc.
L. Gasner, U. Maryland
J. Geffken, DOE-CCU (5)
C. Georgakis, Massachusetts Inst. Technology
R. Glenn, Combustion Processes, Inc.
J. S. Gordon, TRW, Inc., McLean, VA
O. J. Hahn, Univ. Kentucky
W. Hansen, Babcock & Wilcox Co., Barberton, O.
M. J. Hargrove, Combustion Engineering, Inc.
R. D. Harvey, Illinois State Geological Survey
R. Helfenstein, Illinois State Geological Survey
R. G. Hickman, Lawrence Livermore Lab.
F. Hsing, Pratt & Whitney, East Hartford
D. Huber, Burns and Roe, Inc., Paramus, NJ
F. D. Hutchinson, Gibbs and Hill
D. L. Keairns, Westinghouse Research Laboratories
W. E. Kramer, Fluidized Combustion Co.
C. B. Leffert, Wayne State University
A. M. Leon, Dorr-Oliver, Inc.
R. M. Lundberg, Commonwealth Edison Co.
J. J. Markowsky, American Electric Power Service Corp., New York City
M. J. Mayfield, Tennessee Valley Authority, Chattanooga
W. McCurdy, DOE-CCU
J. Mesko, Pope, Evans and Robbins (2)
T. A. Milne, Solar Energy Research Institute
W. G. Moore, Dow Chemical, USA
S. Moskowitz, Curtiss Wright Corporation
W. Norcross, Combustion Engineering, Inc.
T. A. Pearce, Dow Chemical
W. A. Peters, Massachusetts Institute of Technology
C. Petty, Michigan State U.
M. I. Rednicki, Aerojet Energy Conversion, Sacramento
R. Reed, Pope, Evans and Robbins, Inc.
A. F. Sarofim, Massachusetts Institute of Technology
R. D. Smith, Combustion Power Company, Inc.
C. Space, Reynolds, Smith & Hills, Jacksonville, FL
W. K. Stair, Univ. Tennessee
F. Staub, General Electric Corp., Schenectady
W. Steen, U. S. Environmental Protection Agency (16)
M. Steinberg, Brookhaven National Laboratory
W. Strieder, Univ. Notre Dame
S. E. Tung, Massachusetts Institute of Technology

V. Underkoffler, Gilbert Associates, Inc.
W. E. Wallace, Jr., Morgantown Energy Technology Center
F. A. Walton, Combustion Power Co.
A. E. Weller, Battelle Columbus Labs.
T. D. Wheelock, Iowa State University
J. S. Wilson, Morgantown Energy Research Center
K. Yeager, Electric Power Research Inst.
D. Zallen, Energy and Environmental Research Corp., Santa Ana
R. E. Zoellner, Stearns-Roger
J. F. Davidson, U. Cambridge, England
J. Highley, U.K. National Coal Board, England
H. R. Hoy, BCURA Ltd., England
H. Schreckenberg, Bergbau-Forschung GmbH, Germany
G. Moss, Esso Research Centre, England
B. A. Wiechula, Imperial Oil Enterprises, Canada